

# Structural and functional analysis of thiamine- phosphate and homoserine kinases from *Mycobacterium tuberculosis*



UNIVERSITEIT VAN PRETORIA  
UNIVERSITY OF PRETORIA  
YUNIBESITHI YA PRETORIA

Denkleiers • Leading Minds • Dikgopolo tša Dihlalefi

**Clifford Manyo Ntui**

Submitted in partial fulfilment of the degree

*Magister Scientiae* Biochemistry

In the Faculty of Natural and Agricultural Sciences

University of Pretoria

Pretoria

2016-12-21

## **Submission declaration:**

I, Clifford Manyo Ntui, declare that the thesis, which I hereby submit for the Magister Scientiae in the Department of Biochemistry, at the University of Pretoria, is my own work and has not previously been submitted by me for a degree at this or any other tertiary institution.

SIGNATURE.....

DATE.....

## Plagiarism declaration:

**Full name:** Clifford Manyo Ntui      **Student number:** 14334012

**Title of the work:** Structural and functional analysis of thiamine-phosphate kinase and homoserine kinases from *Mycobacterium tuberculosis*

### Declaration

1. I understand what plagiarism entails and am aware of the University's policy in this regard.
2. I declare that this thesis is my own, original work. Where someone else's work was used (whether from a printed source, the internet, or any other source) due acknowledgement was given and reference was made according to the departmental requirements.
3. I did not make use of another student's work and submit it as my own.
4. I did not allow and will not allow anyone to copy my work with the intention of presenting it as his or her own work.

SIGNATURE.....

DATE .....

## Acknowledgements

1. To Dr. Colin Kenyon (CSIR) for providing the plasmid constructs used in this study.
2. The entire Structural Biology group for their support.
3. Professor W-D Schubert for all his overwhelming, especially financial, support.

## Keywords

*Mycobacterium tuberculosis*

Tuberculosis

Thiamine-phosphate kinase

Homoserine kinase

## Abstract

Thiamine-phosphate kinase (or ATP:thiamine-phosphate phosphotransferase, ThiL) and homoserine (ThrB) kinases are essential to metabolism in *Mycobacterium tuberculosis* (Mtb). ThiL and ThrB respectively phosphorylate thiamine monophosphate (TMP) to thiamine diphosphate (TDP), the active form of vitamin B1, and L-homoserine to O-phosphohomoserine, critical to aspartate biosynthesis.

In this study, ThiL and ThrB from Mtb were characterised structurally and functionally by producing the proteins recombinantly in *E. coli*. Proteins were purified by affinity, anion exchange and size exclusion chromatographies and purity checked by SDS-PAGE. ThiL and ThrB enzyme activities were confirmed and reaction products verified by high pressure liquid chromatography (HPLC). The crystal structure of ThiL was solved by molecular replacement using X-ray diffraction data.

Functionally active ThiL, 36 kDa, produced hexagonal crystals belonging to space group P6<sub>1</sub>22 with one monomer per asymmetric unit. Structurally it is related to ThiL from other organisms with minor structural deviations.

Enzymatically active ThrB, 33 kDa, was crystallised. However, crystals failed to diffract X-rays to a suitable resolution. ThiL and ThrB could act as possible anti-TB drug targets against Mtb.

Submission declaration: .....	ii
Plagiarism declaration: .....	iii
Acknowledgements .....	iv
Keywords .....	iv
Abstract .....	v
List of figures .....	ix
List of tables.....	x
List of abbreviations .....	xi
1 Introduction.....	1
1.1 <i>Mycobacterium tuberculosis</i> .....	1
1.1.1 Epidemiology, prevalence and risk factors.....	1
1.1.2 Pathogenesis.....	1
1.1.3 Treatment and possible eventual eradication .....	2
1.1.4 Response and resistance to drugs.....	3
1.1.5 Persistence in the host .....	4
1.2 Kinase.....	5
1.2.1 Structural description .....	5
1.2.2 Occurrence in Mtb.....	6
1.2.3 Thiamine-phosphate kinase (EC 2.7.4.16).....	6
1.2.4 Homoserine kinase (EC 2.7.1.37).....	8
1.3 Aim.....	9
2 Materials and Methods .....	10
2.1. Materials.....	10
2.1.1. Chemicals.....	10
2.1 Enzymes, kits and substrates.....	10
γ-Imino-ATP .....	10
2.1.5 Equipment .....	11
2.1.6 Plasmids.....	12
2.1.8 Buffers .....	13
2.1.9 Culture media .....	14
2.2 Methods.....	14
2.2.1 Molecular biology.....	14

2.2.2 Isolation and digestion of plasmid DNA .....	14
2.2.3 Preparation of glycerol stocks .....	15
2.2.4 Recombinant protein production .....	16
2.2.5 Purification of thiamine-phosphate kinase and homoserine kinase .....	16
2.2.6 Affinity chromatography .....	16
2.2.7 Ni-NTA affinity chromatography .....	16
2.2.8 Protein analytical methods.....	17
2.2.9 SDS-polyacrylamide gel electrophoresis (SDS-PAGE).....	17
2.2.10 Concentration determination.....	18
2.2.11 Anion exchange chromatography .....	18
2.2.12 Size exclusion chromatography.....	19
2.2.13 Functional analysis with thiamine-phosphate kinase .....	19
2.2.14 Functional analysis with homoserine kinase .....	20
2.2.15 Protein crystallization – finding lead conditions .....	20
2.2.16 Optimisation of crystallisation conditions for thiamine-phosphate kinase.....	21
2.2.17 Optimisation of crystallisation conditions for homoserine kinase .....	22
3 Results.....	24
3.1 Restriction digest of ThrB-pET20b and ThiL-pET28a plasmids.....	24
3.2 Protein production and purification.....	24
3.2.1 Production test for His <sub>6</sub> -thiamine-phosphate kinase.....	24
3.2.2 Production and purification of thiamine-phosphate kinase .....	26
3.2.3 Anion exchange chromatography with thiamine-phosphate kinase .....	26
3.2.4 Size exclusion chromatography with thiamine-phosphate kinase.....	27
3.2.5 Production test for homoserine kinase .....	29
3.2.6 Production and purification of homoserine kinase.....	30
3.2.7 Anion exchange chromatography with homoserine kinase.....	30
3.2.8 Size exclusion chromatography with homoserine kinase .....	31
3.3 Functional analysis with thiamine-phosphate kinase .....	32
3.3.1 Analysis of standards .....	33
3.3.2 Analysis of thiamine-phosphate kinase assay component .....	33
3.3.3 Functional analysis with homoserine kinase.....	34
3.3.4 Analysis of homoserine kinase assay component.....	34

3.4	Crystallisation experiments with thiamine-phosphate kinase .....	35
3.4.1	Optimisation of crystallisation conditions for thiamine-phosphate kinase .....	36
3.4.2	pH optimisations .....	36
3.4.3	Precipitant and salt optimisation .....	36
3.4.5	Optimising Crystal Seeding .....	37
3.5	X-ray diffraction, data collection and refinement of thiamine-phosphate kinase	39
3.5.1	Crystal structure of <i>Mycobacterium tuberculosis</i> thiamine-phosphate kinase .	40
3.6	Crystallisation of homoserine kinase .....	43
3.6.1	Optimisation .....	43
4	Discussion .....	45
4.1	Production and purification of thiamine-phosphate and homoserine kinases ....	45
4.2	Functional analysis with thiamine-phosphate kinase (ThiL) .....	46
4.3	Functional analysis with homoserine kinase .....	46
4.4	Crystallisation experiments with thiamine-phosphate kinase .....	46
4.5	Overall structure of <i>Mycobacterium tuberculosis</i> thiamine-phosphate kinase ...	47
4.6	Superposition of MtbThiL with other ThiL structures .....	50
4.7	ATP and TMP sub-sites .....	51
4.8	Crystallisation experiment with homoserine kinase .....	53
5	Conclusion .....	53
6	Outlook .....	54
	References .....	55



## List of figures

- Figure 1.1 Parts of the body affected by TB
- Figure 1.2 Ribbon structure of the overall fold of kinases
- Figure 1.3 Thiamine diphosphate biosynthetic pathway
- Figure 1.4 Schematic diagram of the aspartic pathway of amino acid biosynthesis.
- Figure 2.1 Phosphorylation reaction catalysed by ThiL
- Figure 2.2 Phosphorylation reaction catalysed by ThrB
- Figure 3.1 1% agarose gel of ThrB-pET20b and ThiL-pET28a restriction digestion
- Figure 3.2 15% SDS-PAGE of ThiL production test
- Figure 3.3 15% SDS-PAGE of ThiL after production and Ni-NTA purification
- Figure 3.4 Chromatogram of AXC with ThiL
- Figure 3.5 Chromatogram of SEC with ThiL
- Figure 3.6 15% SDS-PAGE of ThrB production test
- Figure 3.7 15% SDS-PAGE of ThrB after production and Ni-NTA purification
- Figure 3.8 Chromatogram for AXC with ThrB
- Figure 3.9 Chromatogram for SEC with ThrB
- Figure 3.10 Chromatogram from HPLC showing different standards at 200 nm
- Figure 3.11 Chromatogram obtained from HPLC with ThiL assay reaction
- Figure 3.12 Chromatogram obtained from HPLC with ThrB assay reaction
- Figure 3.13 Crystals obtained from initial screening with ThiL
- Figure 3.14 Crystals obtained from pH optimisation with ThiL
- Figure 3.15 Crystals obtained from precipitant and salt optimisation with ThiL
- Figure 3.16 Seeding optimisation with ThiL
- Figure 3.17 X-ray diffraction pattern obtained from ThiL crystal
- Figure 3.18 The overall structure of MtbThiL
- Figure 3.19 Crystals obtained from screening with ThrB
- Figure 3.20 Crystals obtained from optimization with ThrB
- Figure 4.1 Structural topology of MtbThiL with other ThiL structures
- Figure 4.2 Sequence alignment of MtbThiL with selected ThiL proteins

Figure 4.3 Superposition of MtbThiL with other ThiL structures

Figure 4.4 Close-up view of ATP and TMP active sub-sites

## List of tables

Table 1.1 Summary of the molecular mechanisms of anti-TB drug resistance

Table 2.1 List of enzymes, kits and substrates

Table 2.2 Equipment used

Table 2.3 Plasmids used

Table 2.4 Buffers used

Table 2.5 Culture media used

Table 3.1 Purification table for ThiL

Table 3.2 Purification table for ThrB

Table 3.3 Summary of data collection statistics for ThiL crystal

Table 3.4 Summary of refinement statistics for ThiL crystal

## List of abbreviations

A <sub>260</sub>	Absorbance at 260 nm
ADP	Adenosine diphosphate
AhpC	Alkyl hydroperoxide reductase protein C
ATP	Adenosine triphosphate
AXC	Anion exchange chromatography
bp	Base pair
CV	Column volume
CSIR	Council for Scientific and Industrial Research (South Africa)
Da	Dalton
DTT	1,4-Dithiothreitol
ESRF	European Synchrotron Radiation Facility
FPLC	Fast pressure liquid chromatography
FurA	Ferric uptake regulation protein A
GHMP	Galacto, homoserine, melavonate and phosphomelavonate kinases
GyrA	Gyrase A protein
GyrB	Gyrase B Protein
h	Hour(s)
HPLC	High pressure liquid chromatography
His <sub>6</sub>	Hexa-histidine
IPTG	Isopropyl β-D-thiogalactoside
kDa	Kilo-Dalton
mAU	Milli absorbance units (relative value)
MDR-TB	Multidrug-resistant tuberculosis
Mtb	<i>Mycobacterium tuberculosis</i>
Ni-NTA	Nickel-nitrilotriacetic acid
OD	Optical density
PAGE	Polyacrylamide gel electrophoresis
PCR	Polymerase chain reaction

PCR-RFLP	PCR-restriction fragment length polymorphism
PDB	Protein Data Base
pI	Isoelectric point
RMS	Root mean square
RNA	Ribonucleic acid
SDS	Sodium dodecyl sulphate
SDS-PAGE	Sodium dodecyl sulphate polyacrylamide gel electrophoresis.
SEC	Size exclusion chromatography
TB	Tuberculosis
TDP	Thiamine diphosphate
ThiL	Thiamine-phosphate kinase
ThrB	Homoserine kinase
ThiL-pET28a	ThiL-pET28a plasmid
ThrB-pET20b	ThrB-pET20b plasmid
TMP	Thiamine monophosphate
TPK	Thiamine pyrophosphokinase
UV	Ultraviolet
XDR-TB	Extensively drug-resistant tuberculosis
WHO	World Health Organisation

# 1 Introduction

## 1.1 *Mycobacterium tuberculosis*

*Mycobacterium tuberculosis* (Mtb) is a non-motile, acid fast, obligate aerobe characterized by mycolic acids in its outer cell wall and a very slow generation time of between 10 and 20 h (Palsson-Mcdermott and O'Neill, 2004). In 1882, Robert Koch identified Mtb as the causative agent of tuberculosis (TB) (Koch, 1882). Despite more than a century having passed since, Mtb still kills millions of humans worldwide every year (Cadena et al., 2016).

### 1.1.1 Epidemiology, prevalence and risk factors

TB as a disease remains a major global health problem, with thousands of new infections every day. The WHO reported about nine million cases of active TB for 2015 and 1.5 million deaths (WHO, 2016). The highest rates of Mtb infection are observed in sub-Saharan Africa, India and China linked to poor nutrition, inadequate medical care, crowding, unemployment and low levels of education (WHO, 2016).

Risk factors such as smoking, alcohol and drug abuse increase infection rates (Lönnroth et al., 2009). Age and gender are also critical parameters, with young adults in developing countries showing the highest rate of TB. In developed countries, by contrast, the elderly are most affected (Kwon *et al.*, 2013).

### 1.1.2 Pathogenesis

Mycobacteria are transmitted by air-borne droplets from patients with acute TB (Fernstrom and Goldblatt, 2013). When another person inhales these droplets, the mycobacteria will predominantly infect the lungs. However, other parts of the body may also be affected such as the middle ear, adrenal glands, tonsils, etc. (Figure 1.1) (Pai et al., 2016).

Upon reaching the lungs of an infected individual, mycobacteria are engulfed by macrophages. Other immune cells will surround the infected macrophages forming a granuloma that encapsulates the mycobacteria and prevents them from spreading (Podinovskaia et al., 2013).

TB is classified as either “active” or “latent” depending on the ability of the immune system to control the disease (Getahun et al., 2015). A well-functioning immune system will restrict mycobacteria into a dormant state inside granulomata leading to so-called latent infections. Tuberculous lesions will be present but the host will not portray

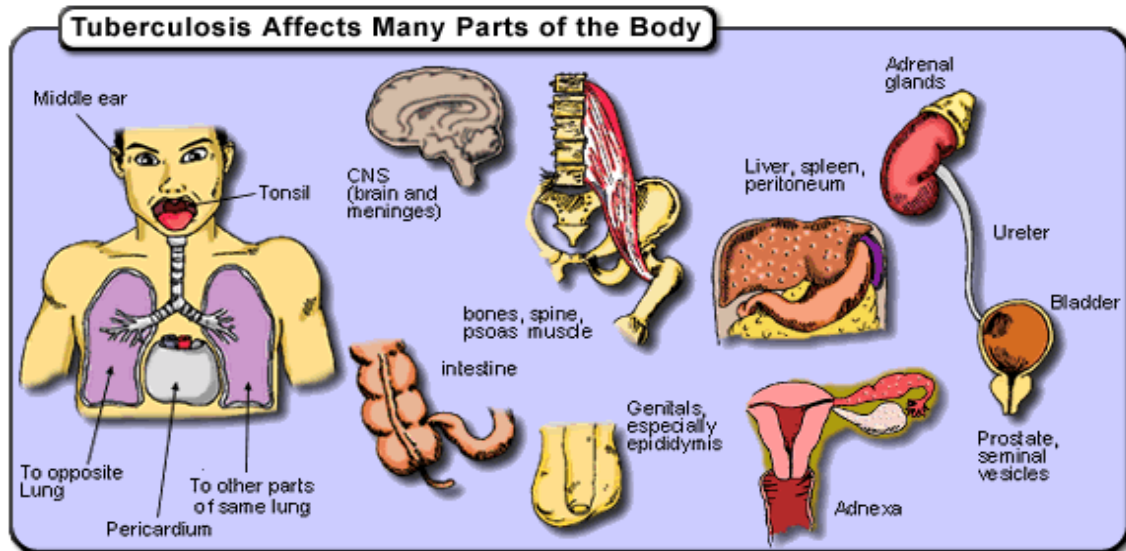


**Figure 1.1: Parts of the body potentially affected by TB.** After the primary infection of the lungs, Mtb may spread to other parts of the body such as the middle ear, tonsil and liver (adapted from [www.wuth.nhs.uk](http://www.wuth.nhs.uk)).

symptoms of the disease. An apparently healthy individual may thus carry latent mycobacteria for extended periods. When the host immune system is impaired, patients develop active TB characterized by chest pain, pneumonia and a persistent, often bloody cough. Lymph nodes may become enlarged, especially around the lungs and heart (Hui et al., 2015). Mycobacteria will actively grow and divide, and may spread. They can only be detected and cultured in active TB.

### 1.1.3 Treatment and possible eventual eradication

The complete elimination of mycobacteria from an individual is a slow and arduous process. The WHO and governments have committed to control or eventually eradicate TB by ensuring a regular supply of TB drugs, developing new treatment strategies for multidrug resistant TB, reversing the rising incidence of TB by 2015, improving TB diagnosis, prevention and treatment tools to reduce worldwide TB incidence to less than 1 per million by 2050 (Houben and Dodd, 2016).

#### 1.1.4 Response and resistance to drugs

The fight against TB has made some gains over the past few years. The progress is, however, being threatened by drug-resistant TB which is assumed to develop when patients fail in their drug compliance (Caminero *et al.*, 2010). Drug-sensitive TB, by contrast, refers to TB that is treatable with any, especially first-line TB drug (Gillespie *et al.*, 2014).

Attempts to produce effective anti-TB drugs or vaccines have been largely unsuccessful. First-line drugs such as isoniazide, rifampicin, rifapenline, pyrazinamide, streptomycin, and ethambutol provided some relief in the fight against drug-sensitive TB (Bhutani *et al.*, 2005). They need to be taken for several months and have an efficacy of more than 90% with few side effects noted in the recipients (Petrini and Hoffner, 1999). This relief was, however, only temporary, following the emergence of multidrug-resistant tuberculosis (MDR-TB) with resistance to rifampin and isoniazide (Velayati *et al.*, 2009). Second-line drugs such as viomycin, fluoroquinolones, ofloxacin, ciprofloxacin, D-cycloserine, kanamycin, amikacin, ethionamide, and aminoglycosides help against MDR-TB but require longer treatment periods, have more side effects and a higher price-tag than first-line drugs (Orenstein *et al.*, 2009). Resistance to second-line drugs in MDR-TB complicates treatment further (Zemlyanaya *et al.*, 2015).

Extensively drug-resistant tuberculosis (XDR-TB) involves Mtb strains resistant to rifampin and isoniazide as well as second-line drugs fluoroquinolones and capreomycin. Recent anti-TB drugs such as diarylquinoline and nitroimidazoles are effective against both drug-sensitive and drug-resistant Mtb strains, but again resistances have resulted (Cdc, 2006).

Drug resistance mechanisms in Mtb have been investigated using modern molecular methods. Mutation detection methods include PCR-RFLP, molecular DNA sequencing and heteroduplex analysis (Zhang and Yew, 2009a). Molecular epidemiological methods have been instrumental in identifying clusters of drug resistance in TB as well as the underlying mutations (Table 1.1) with codon mutations most commonly causing TB drug resistance (Song *et al.*, 2015). Resistance to rifampin and ethambutol, for example, are linked to mutations in the genes *rpoB* and *embB* respectively (Kardan Yamchi *et al.*, 2015).

Protein phosphorylation by kinases also contribute to drug resistance in TB (Molle *et al.*, 2010), (Lee *et al.*, 2014) while kanamycin kinase phosphorylates kanamycin, reducing its

effectiveness against TB (Metri *et al.*, 2015). **Table 1.1: Summary of the molecular mechanisms of anti-TB drug resistance** (Palomino and Martin, 2014)

Drug	Associated mutated gene	Associated protein from Mtb
Rifampin	rpoB	B-subunit of RNA polymerase
	ahpC	AhpC
	furA	FurA
Streptomycin	rrS	Ribosomal RNA 16S protein
	rpsL	Ribosomal RNA 30S protein
Pyrazinamide	pncA	pyrazinamidase
Ethambutol	embB	EmbB protein
Fluoroquinolones	gyrA	GyrA protein
	gyrB	GyrB Protein

TB drug resistances in humans often develop when patients fail to complete treatment as most anti-TB drugs are administered over a period of six months allowing mycobacteria to adapt to the drug (Zhang and Yew, 2009b). Lack of effective TB control programs and poverty in developing countries are thus major concerns.

#### 1.1.5 Persistence in the host

Mtb can withstand oxidative agents, toxins, and can survive low nutrient conditions (Gengenbacher and Kaufmann, 2012). To fight pathogens, an initial host immune response is to recruit macrophages to engulf and kill the pathogen through reactive oxygen and nitrogen intermediate production as well as phago-lysosomal fusion (Sia *et al.*, 2015). To survive this onslaught, Mtb detoxifies reactive oxygen and nitrogen species (Weiss and Schaible, 2015a). In addition, glycosylate cycle enzymes channel carbon from fatty acid  $\beta$ -oxidation to the glycosylate pathway to sustain a nutrient starved intracellular infection (Lee *et al.*, 2015). Induction of the gluconeogenesis and glycosylate



shunt genes has been shown to be active during nutrient deprivation (Ehrt *et al.*, 2015). In addition, genes involved with the production of RNA and transcription are induced. During induction of these genes, other pathways such as those involved in *de novo* ATP and nucleobase synthesis are down-regulated (Gengenbacher and Kaufmann, 2012). This gene regulation allows the mycobacteria to persist in nutrient deprived environment.

Mtb cells also encounter stressors such as antimicrobial agents and toxic radicals within the host which are frequently detrimental to their DNA (Weiss and Schaible, 2015b). The mycobacteria are able to activate DNA repair mechanisms to protect the integrity of their genome. A conserved DNA glycosylase involved in DNA repair has been found in mycobacteria (Guo *et al.*, 2010).

Regulatory mechanisms through protein-protein interaction are believed to be crucial in the persistence of Mtb (Prisic *et al.*, 2010). Amongst the most studied gene regulatory pathways in Mtb is the phosphorylation pathway (Baer *et al.*, 2014). This pathway, catalysed by serine/threonine protein kinase is involved in many Mtb gene regulatory processes (Lee *et al.*, 2014). Some of the 11 Mtb protein kinase discovered so far are known to be crucial in protein phosphorylation (Prisic and Husson, 2014).

The current state of Mtb (its drug resistance and persistence in the host), has prompted the need for the development of more effective drugs and possible vaccines against TB. Therefore, targeting alternative biosynthesis pathways can provide the solution to TB drug resistance and the persistence of Mtb in the host.

## **1.2 Kinase**

### **1.2.1 Structural description**

Protein and non-protein kinases share a similar protein fold (figure 1.2). They vary in their core sequences and flanking regions allowing each to bind a unique substrate and to respond to distinct activation and inhibition signals (Nolen *et al.*, 2004). Phosphate transfer generally involves a divalent metal ion, mostly  $Mg^{2+}$ .

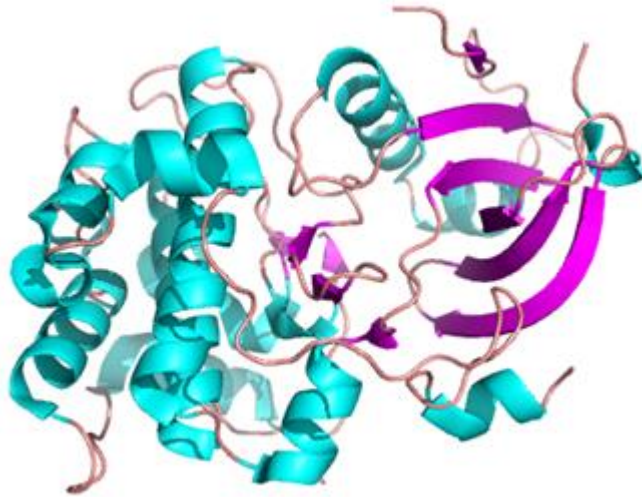


**Figure 1.2: Cartoon structure of Akt kinase as an example of a typical kinase fold.**

Kinases share a similar fold comprised of two lobes. The first mainly consists of a  $\beta$ -sheet (magenta), the other of  $\alpha$ -helices (cyan). These lobes structure form an ATP binding cleft that constitutes the active site. The coordinates **3CQU** were downloaded from the Protein Data Base (PDB). The figure was prepared using PyMol.

### 1.2.2 Occurrence in Mtb

Living cells perceive environmental signals and respond to these through signal transduction pathways (Sih *et al.*, 2011) often involving reversible phosphorylation (Humphrey *et al.*, 2015, (Fischer, 2013). Serine/threonine/tyrosine phosphorylation in eukaryotes is well understood (Pereira *et al.*, 2011, (Grangeasse *et al.*, 2007). However, much less so in prokaryotes such as Mtb. Bacteria often have complex lifestyles and kinases are essential in their adaptation, development and virulence (Grangeasse *et al.*, 2012).

Mtb has both non-protein and 11 protein kinases most of which are uncharacterised. Mtb kinases remaining to be characterised in detail include thiamine-phosphate kinase (ThiL) and homoserine kinase (ThrB). These kinases are essential in Mtb metabolism and may thus constitute drug targets to fight TB.

### 1.2.3 Thiamine-phosphate kinase (EC 2.7.4.16)

All organisms hydrolyse extracellular thiamine phosphate to thiamine before uptake. Intracellularly, thiamine is pyrophosphorylated to thiamine pyrophosphate by thiamine

pyrophosphokinase (TPK, (Tian *et al.*, 2016, (Hayashi and Nosaka, 2015). Thiamine naturally occurs in four forms: free thiamine, thiamine-phosphate, thiamine pyrophosphate and thiamine triphosphate (Ihara *et al.*, 2005). Eukaryotes mostly obtain thiamine from their diet, while bacteria and yeast synthesize it themselves. Dietary thiamine is phosphorylated by ThiL or pyrophosphorylated by TPK (Hayashi and Nosaka, 2015). However, note that ThiL has been used unspecifically to refer to a number of different thiamine kinases, including thiamine kinase (EC 2.7.1.89), thiamine phosphate kinase (EC 2.7.4.16) and thiamine diphosphate kinase (EC 2.7.4.15) leading to much confusion in the literature. In fact, ThiL only phosphorylates thiamine phosphate to thiamine diphosphate (figure 1.3). The latter is the active form of vitamin B1 and a coenzyme for glucose metabolism in Mtb (Du *et al.*, 2011). Other common names for thiamine-phosphate kinase are thiamine pyrophosphatase, thiamine monophosphate kinase and thiamine monophosphokinase.

Currently, only ThiL enzymes from *Aquifex aeolicus*, *Acinetobacter baumannii* and *Methylobacillus flagellatus* have been structurally investigated.

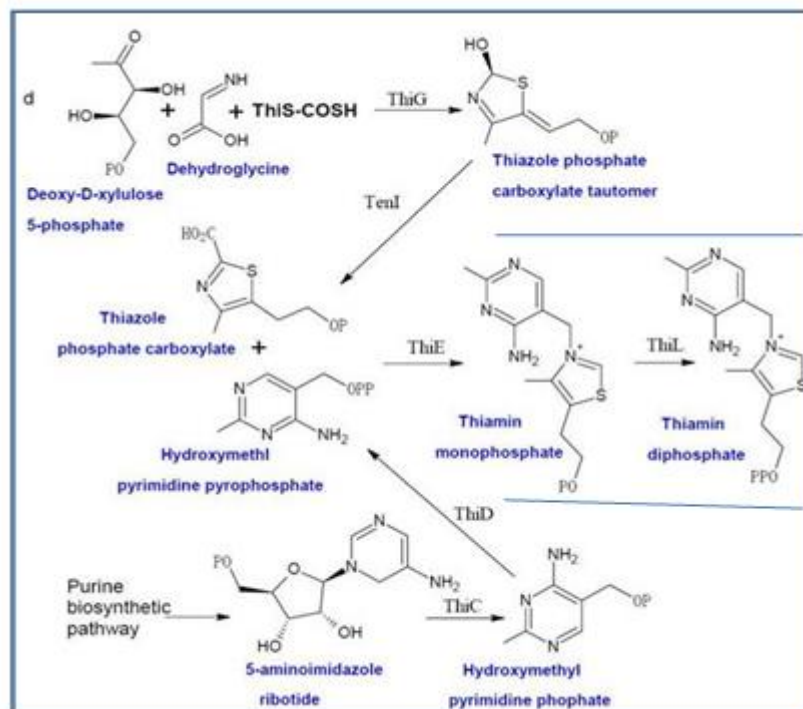


**Figure 1.3: Thiamine diphosphate biosynthesis:** ThiL catalyses the ATP-dependent phosphorylation of thiamine monophosphate (TMP) to thiamine diphosphate (TDP) or

active vitamin B1 (adapted from (Du et al., 2011).

### 1.2.4 Homoserine kinase (EC 2.7.1.37)

Homoserine kinase (ThrB) is a kinase that participates in aspartate biosynthesis (figure 1.4) (Zhou *et al.*, 2000). ThrB belongs to the common GHMP (galactose, homoserine, melavonate and phosphomelavonate) kinase family (Yang *et al.*, 2002). ThrB catalyses the phosphorylation of L-homoserine to L-homoserine phosphate, an intermediate in the production of L-threonine, L-isoleucine, and L-methionine. ThrB is essential in the cellular function of most organisms (Kingsbury and Mccusker, 2010). In some pathogenic microorganisms such as *Listeria monocytogenes* and Mtb, homoserine is involved in ensuring survival during adverse conditions (Ferla and Patrick, 2014, (O'barr and Everett, 1971). High levels of L-homoserine inhibit the activity of ThrB in *E. coli*, but not in plants and archaea (Rees *et al.*, 1992, (Theze *et al.*, 1974). ThrB is also inactivated by chemicals such as pyridoxal phosphate and diethylpyrocarbonate due to loss of a histidine residue (Rees *et al.*, 1992).

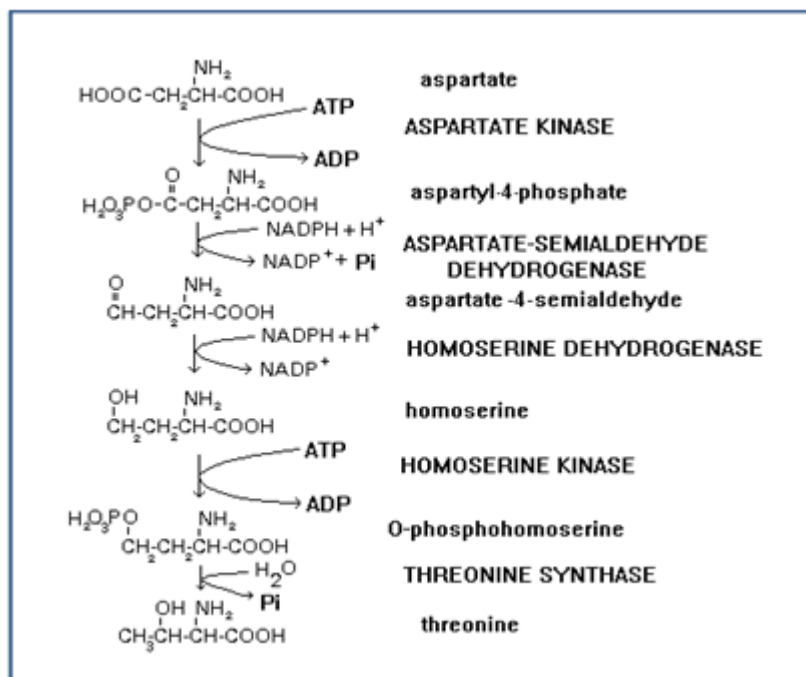


**Figure 1.4: The conversion of aspartate to threonine.** ThrB is an enzyme in the metabolic pathway from aspartate to threonine. ThrB phosphorylates homoserine to O-phosphohomoserine using ATP (adapted from Xu et al., 2013).

Crystal structures have been solved for ThrB from a number of organisms. These include *Agrobacterium tumefaciens*, *Listeria monocytogenes*, *Methanococcus jannaschii* and *Pseudomonas aeruginosa*. The structure from *M. jannaschii* revealed a unique kinase fold and new nucleotide-binding mode conserved among GHMP kinases (Zhou *et al.*, 2000). No crystal structure of Mtb ThrB has been reported, limiting our understanding of its structural details and mechanism of action.

### **1.3 Aim**

ThiL and ThrB are critical for Mtb metabolism, justifying a more detailed characterisation of these enzymes including at a structural level. ThiL and ThrB from Mtb were produced as recombinant His<sub>6</sub>-fusion proteins in *E. coli*. Recombinant proteins were purified using affinity, ion exchange and size exclusion chromatographies. The enzymes were functionally analysed by kinase assays. The proteins were crystallised by hanging-drop, vapour-diffusion and the structure was solved by the molecular replacement.

## 2 Materials and Methods

### 2.1. Materials

#### 2.1.1. Chemicals

Unless otherwise stated, suppliers of chemicals and reagents used for this project are as follows: Biolab, Fermentas, GE Healthcare Life Sciences, Inqaba Biotech, Invitrogen, Merck Millipore, Novagen, Promega, Qiagen, Roche, Sigma Aldrich, Stratagene and Thermo Scientific.

#### 2.1 Enzymes, kits and substrates

**Table 2.1: List of enzymes, kits and substrates**

Restriction enzyme	Description	Supplier
XhoI		New England Biolabs (Ipswich, UK)
NdeI		
<b>Kits</b>		
GeneJET™ Plasmid Mini-Prep Kit		Fermentas (Burlington, Ontario, Canada)
<b>Substrates</b>		
L-Homoserine		Sigma Aldrich (St. Louis, Missouri, USA)
TMP		
ATP		
ADP		
γ-Imino-ATP		
<b>Molecular weight standards</b>		
Smart Ladder	DNA Marker 200-10000 bp	Fermentas (Burlington, Ontario, Canada)
Unstained Protein Ladder	Protein Marker 14.4 to 116 kDa	
<b>Crystallization screens</b>		
The (NH <sub>4</sub> ) <sub>2</sub> SO <sub>4</sub> Suite		Qiagen (Germantown, Wisconsin, USA)
The Compas Suite		
The Cryo Suite		
The PACT Suite		
The PEGs Suite		

## 2.1.5 Equipment

**Table 2.2: Equipment used in the study**

Equipment	Model	Supplier
Autoclave	J.S.D. 400	HOSPI (Chatsworth, California, USA)
Centrifuges	Sorvall® RC6	Thermo Scientific (Waltham, Massachusetts, USA)
	Megafuge 8R	Thermo Scientific (Waltham, Massachusetts, USA)
	5417C	Eppendorf (Hamburg, Germany)
Centrifugal filter Units	Amicon® Ultra-15	Merck Millipore (Billerica, Massachusetts, USA)
Chromatography columns	10 ml Column, 35 µm filter pore size gravity flow column	MoBiTech (Goettingen, Germany)
	Mono Q 10/100 GL	GE Healthcare (Boston, Massachusetts, USA)
	Superdex 200 10/300 GL	
	Hypersil GOLD column	Thermo Scientific (Waltham, Massachusetts, USA)
Protein concentrator	Vivaspin	Merck Millipore (Billerica, Massachusetts, USA)
Digital Camera	DP11	Olympus (Tokyo, Japan)
Electrophoresis Chamber	Power Pac™ Basic	Bio-Rad (Hercules, California, USA)
Electrophoresis Power Pack		
FPLC System	ÄKTAbasic 900	GE Healthcare (Boston, Massachusetts, USA)
HPLC	Ultimate 3000, Dionex	Thermo Scientific (Waltham, Massachusetts, USA)
Microscopes	KEYENCE LEICA DFC320 digital microscope	Keyence corporation (Osaka, Japan)
	Zeiss discovery .V8 microscope	Zeiss (Oberkochen, Germany)
Mosquito nanolitre crystallisation robot	PK243 – 01A	TTP labtech (Cambridge, UK)
Nanodrop Photometer	ND-1000 Spectrophotometer	PEQLAB (Erlangen, Germany)
pH Meter	CRISON	Lasec (Johannesburg, South Africa)
Shaker (Roller)	Roller Mixer SRT6	Stuart Scientific (Stone, UK)
Shaking Incubator	Multitron II	INFORS (Bottmingen, Switzerland)

Sonicator	Qsonica	Lasec (Johannesburg, South Africa)
Water purification system	Milli - Q	Merck Millipore (Billerica, Massachusetts, USA)

### 2.1.6 Plasmids

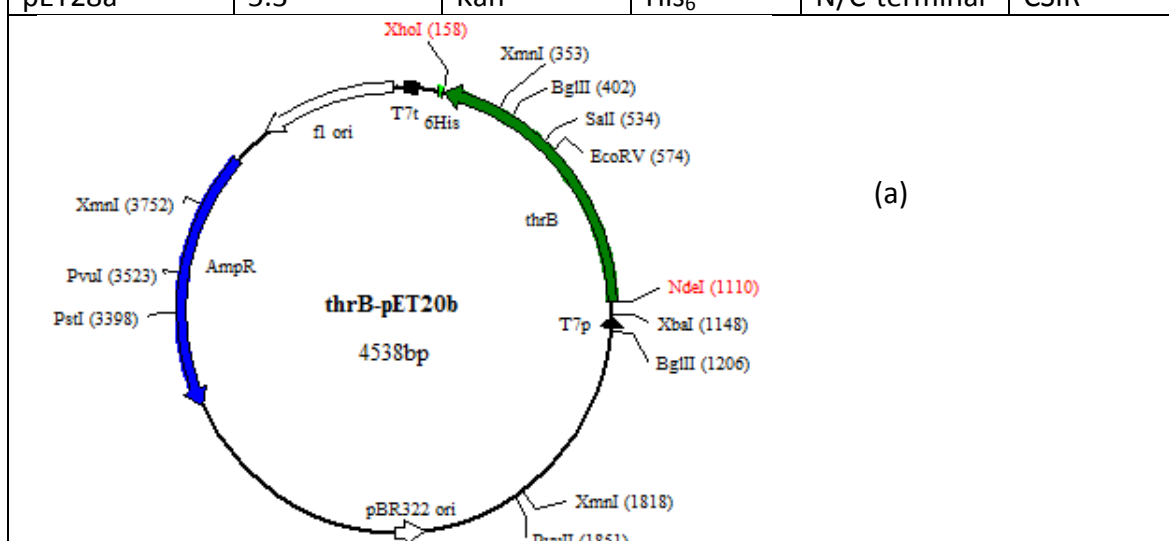
#### pET28a

pET28a is a bacterial expression vector encoding both an N-terminal and a C-terminal His<sub>6</sub>-tag. Expression is under the control of the T7 *lac* promoter induced by the lactose analogue isopropyl β-D-thiogalactoside (IPTG) (Novagen, Billerica, USA).

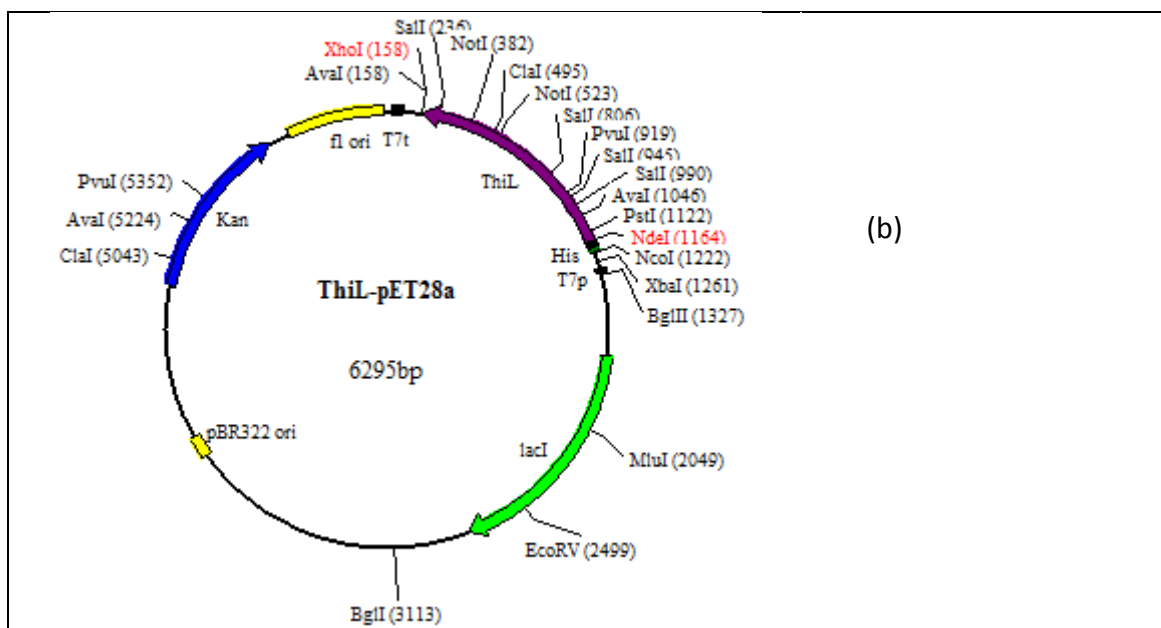
#### pET20b

pET20b is a bacterial expression vector that carries an N-terminal pelB signal sequence for periplasmic localization, plus an optional C-terminal His<sub>6</sub>-tag. Expression is under the control of the T7 *lac* promoter induced by IPTG (Novagen, Billerica, USA).

**Table 2.3: Recombinant plasmids used**

Plasmid	Size (Kb)	Selection	Tag	Position	Supplier
pET28a	5.3	Kan <sup>R</sup>	His <sub>6</sub>	N/C-terminal	CSIR
					
pET20b	3.7	Amp <sup>R</sup>	His <sub>6</sub>	C-terminal	CSIR





(b)

### 2.1.8 Buffers

Unless otherwise stated, buffers used for this study are listed below.

**Table 2.4: Buffers used**

Buffers/Solutions	Constituents
TAE buffer	40 mM Tris-HCl pH 7.5, 20 mM sodium acetate, 1 mM EDTA adjusted pH to 8.2 with acetic acid
10 x DNA loading buffer	70% (w/v) sucrose, 0.25% (w/v) bromophenol blue, 0.1 M EDTA
Ni-NTA lysis buffer	0.5 M NaCl, 30 mM imidazole, 20 mM Tris-HCl pH 7.9
Ni-NTA wash buffer	0.25 M NaCl, 40 mM imidazole, 20 mM Tris-HCl pH 7.9
Ni-NTA elution buffer	0.5 M NaCl, 250 mM imidazole, 20 mM Tris-HCl pH 7.9
SDS-PAGE lower buffer (4 x)	1.5 M Tris-HCl pH 8.8
SDS-PAGE upper buffer (4 x)	0.5 M Tris-HCl pH 6.8, 0.4% (w/v) SDS
SDS-PAGE running buffer	25 mM Tris-HCl pH 7.9, 192 mM glycine, 0.1% (w/v) SDS
SDS-PAGE sample buffer (8 x)	16 mL 10% SDS, 4 mL glycerol, 2.2 mL Tris-HCl pH 6.8, 800 $\mu$ L mercaptoethanol, 1 spatula tip bromophenol blue

SDS-PAGE separating gel (15%)	15 mL acrylamide 30% (w/v), 7.6 mL 1.5 M Tris-HCl pH 6.8, 300 $\mu$ L 10% (w/v) SDS, 10 mL ddH <sub>2</sub> O, 40 $\mu$ L TEMED, 100 $\mu$ L 2% (w/v) APS
SDS-PAGE stacking gel (5%)	1.5 mL acrylamide, 30% (w/v), 2.5 mL 0.5 M Tris-HCl pH 6.8, 5.9 mL ddH <sub>2</sub> O, 15 $\mu$ L TEMED, 25 $\mu$ L 25% (w/v) APS
SDS-PAGE Staining solution	0.25% (w/v) Coomassie Brilliant Blue R-250, 30% (v/v) ethanol, 10% (v/v) acetic acid
SDS-PAGE destaining solution	40% (v/v) ethanol, 10% (v/v) acetic acid
Buffer A (for ion exchange chromatography)	25 mM NaCl, 25 mM Tris-HCl pH 8.0
Buffer B (for ion exchange chromatography)	1 M NaCl, 25 mM Tris-HCl pH 8.0

### 2.1.9 Culture media

The following culture media were used for this study.

**Table 2.5: Culture media used**

Culture media	constituents
Lysogeny Broth (LB medium)	10 g/L bactotryptone, 5 g/L yeast extract, 5 g/L NaCl
LB-Ampicillin-Medium	LB-medium plus 100 $\mu$ g/mL Ampicillin
LB-Kanamycin-Medium	LB-medium plus 50 $\mu$ g/mL Kanamycin

All media were autoclaved for 20 min at 121°C before use.

## 2.2 Methods

### 2.2.1 Molecular biology

#### 2.2.2 Isolation and digestion of plasmid DNA

For this study, freshly transformed *E. coli* BL21 (DES) colonies containing ThiL-pET28a and ThrB-pET20b (Dr. Colin Kenyon, CSIR) were used. To confirm the presence of *thiL* and *thrB* genes in their respective plasmids, the latter were extracted and double digested with XhoI and NdeI restriction endonucleases.

### **Isolation of plasmid DNA**

A single freshly transformed *E. coli* BL21 (DES) colony containing ThiL-pET28a or ThrB-pET20b was picked and transferred to 5 mL LB-medium with the required antibiotic. The culture was allowed to grow at 37°C overnight in a shaker incubator. A Qiagen mini prep kit (GeneJET plasmid) was used to isolate and purify plasmid DNA according to the manufacturer's instructions.

### **Determination of plasmid DNA concentrations**

DNA concentrations were determined spectrophotometrically by measuring the absorbance at 260 nm ( $A_{260}$ ) and 280 nm ( $A_{280}$ ) on a ND-1000 NanoDrop. The spectrophotometer was blanked with 2  $\mu$ L reference buffer and 2  $\mu$ L DNA sample was then used to take the concentration and recorded.

### **Digestion of plasmid DNA**

Restriction enzymes recognise specific nucleotide sequence in double-stranded DNA and specifically cleave these. Most enzymes recognise palindromic sequence and produce either blunt or sticky ends (Roberts et al., 2003). Sixteen  $\mu$ L of 114 ng/ $\mu$ L ThiL-pET28a (or 125 ng/ $\mu$ L ThrB-pET20b) were transferred to a PCR tube on ice. Similarly, 5  $\mu$ L restriction buffer (10 x) and 1  $\mu$ L each of XhoI and NdeI were added. The final volume was made up to 50  $\mu$ L with ddH<sub>2</sub>O. The tubes were incubated at 37°C for 1 h and samples were analysed by agarose gel electrophoresis. Presence of the *thiL* and *thrB* gene inserts was confirmed by sequencing at the University of Pretoria sequencing facility, South Africa.

### **2.2.3 Preparation of glycerol stocks**

Glycerol is added to bacterial cells containing a plasmid of interest to prevent the cells from lysing during the freezing process allowing their long term storage (Kurachi et al., 2014). Glycerol stocks for ThiL-pET28a and ThrB-pET20b were separately prepared by inoculating 5 mL LB-medium plus relevant antibiotic with bacteria containing the respective recombinant plasmid. The culture was incubated overnight at 37°C and a rotation speed of 150 rpm. In a 1 mL cryovial, 100  $\mu$ L of sterile 80% (v/v) glycerol and 900  $\mu$ L of the overnight culture were combined and gently mixed for storage at -80°C.

#### **2.2.4 Recombinant protein production**

Cells from the glycerol stocks harbouring the ThiL-pET28a were inoculated into 20 mL LB-medium containing 50 µg/mL kanamycin antibiotic and grown overnight at 37°C and 160 rpm. The culture was transferred to 1 L LB-medium containing 1 mL 50 µg/mL kanamycin antibiotic and grown at 37°C and 180 rpm to an OD<sub>600</sub> of 0.5 to 0.8. Protein production was induced with 0.1 M IPTG and continued at 22°C with 180 rpm shaking overnight. Before and after induction, 1 mL of the cell culture was collected, pelleted by centrifugation at 12000 x g for 2 min using the 5417C centrifuge. The pellets were suspended in an equivalent amount of SDS sample buffer to lyse the cells depending on the OD<sub>600</sub> to analyse induction of target protein. After overnight incubation, cells were harvested by centrifugation: 15 min, 4°C, 6000 x g using the Sorvall® RC6 centrifuge with the SL3000 rotor. The supernatant was discarded and the cell pellet resuspended in 20 mL lysis buffer per 1 L culture at 4°C. The cells were lysed by sonication on ice using seven 30 s on/off cycles using the sonicator. The lysate was centrifuged for 1 h at 4°C and 16000 x g using the Sorvall® RC6 centrifuge with the SA600 rotor to separate the soluble protein fraction from cell debris and inclusion bodies. Soluble (supernatant) and insoluble (pellet) fractions were collected, 100 µL 8 M urea was added to the pellet fraction (to solubilise proteins) and samples were analysed on SDS-PAGE.

This procedure above was similarly used to produce recombinant ThrB protein from cells harbouring the ThrB-pET20b. The LB-medium was inoculated with ampicillin antibiotic (100 µg/mL).

#### **2.2.5 Purification of thiamine-phosphate kinase and homoserine kinase**

#### **2.2.6 Affinity chromatography**

Affinity chromatography is a purification method based on the high affinity of a molecular tag covalently fused to the N- or C-terminus of a target protein to an immobilized matrix (Urh *et al.*, 2009). ThiL and ThrB were produced with an N-terminal and a C-terminal hexa-histidine (His<sub>6</sub>) tag, respectively.

#### **2.2.7 Ni-NTA affinity chromatography**

Recombinant proteins containing a His<sub>6</sub>-tag may be purified by Ni-NTA (nickel-nitrilotriacetic acid) affinity chromatography. This purification method takes advantage of

the ability of histidine residues to interact with transition metal ions such as nickel ions. The carbonyl group, the imidazole and the amino nitrogen atoms of histidine coordinate the nickel (II) ions to form an octahedral coordination and a bis (histidine) complex is formed at a pH higher than 5. The imidazole group on histidine provides the binding site for nickel ions. These histidine residues bind with very high affinity to nickel ions immobilised on nickel-nitrilotriacetic acid matrix (Bornhorst and Falke, 2000). To remove the His<sub>6</sub>-tag alongside the protein of interest from the matrix, a buffer with high concentration of imidazole (to outcompete the binding of nickel (II) ion on the histidines) is used.

The soluble lysate from centrifugation at 16000 x g was added to Ni-NTA agarose resin pre-equilibrated with lysis buffer in a gravity flow column. This resin was incubated at 4°C for 2 h with mild agitation to allow the target protein to bind. The flow through was collected by gravity flow and a 15 µL sample was analysed on sodium dodecyl sulphate (SDS) polyacrylamide gel electrophoresis (PAGE) to detect unbound fusion protein. The Ni-NTA resin was washed by gravity flow with 500 mL wash buffer which contained 40 mM imidazole to remove untagged proteins, while the protein of interest remain on the resin. Both His<sub>6</sub>-ThiL and His<sub>6</sub>-ThrB fusion proteins were eluted from the Ni-NTA using 30 mL elution buffer containing 200 mM imidazole which competes with the nickel (II) ion for the imidazole binding site on the histidines. Thus His<sub>6</sub>-ThiL and His<sub>6</sub>-ThrB fusion proteins will be eluted from the Ni-NTA resin.

### **2.2.8 Protein analytical methods**

#### **2.2.9 SDS-polyacrylamide gel electrophoresis (SDS-PAGE)**

Sample fractions assumed to contain His<sub>6</sub>-ThiL or His<sub>6</sub>-ThrB fusion proteins were analysed by sodium dodecyl sulphate (SDS) polyacrylamide gel electrophoresis (PAGE), which separates proteins based on their molecular weight. SDS is a strong detergent, that non-covalently binds to proteins, disrupting their native structure and induces an overall negative charge that enables proteins to migrate towards a positively charged anode in an electric field (Gallagher, 2001). Fifteen µL protein samples were mixed with 5 µL of 6 x sample buffer and heated at 95°C for 5 min to denature the protein. The protein samples were loaded onto the gel and run at 40 mA for 20 to 30 min. The gel was stained for 30 min in a Coomassie Brilliant Blue R-250 solution. Destaining solution was used to remove excess stain.

### 2.2.10 Concentration determination

Proteins samples were concentrated for further purification and downstream experiments (activity assay and crystallisation) by ultracentrifugation using Vivaspin concentrators with a molecular weight cut-off at least 10 kDa smaller than the protein. The concentration of purified proteins was measured by measuring the absorbance at 280 nm using a Nanodrop ND-1000 spectrophotometer.

### 2.2.11 Anion exchange chromatography

To ensure sufficient purity of His<sub>6</sub>-ThiL and His<sub>6</sub>-ThrB fusion proteins for downstream experiments, both proteins were further purified by anion exchange (AXC) and size exclusion chromatographies (SEC).

In AXC biomolecules are separated by differences in their net surface charge allowing molecules with small differences in charge to be separated (Hansen, 2015). The net surface charge of biomolecules is affected by the surrounding pH. The net surface charge of amphoteric proteins changes gradually with the surrounding pH (Selkirk, 2004). At a pH below its isoelectric point (pI), a protein has a net positive surface charge and binds to a negatively charged matrix (cation exchanger), and *vice versa* above its pI. Bound proteins are eluted by passing a buffer of increasing ionic strength or changing pH through the material (Hansen, 2015). The pI of ThiL and ThrB are 5.6 and 5.5, respectively. Both proteins were purified using anion exchanger.

A Mono Q 10/100 GL column connected to an ÄKTAbasic 900 fast pressure liquid chromatography (FPLC) machine was used for AXC. The column was equilibrated with 5 column volumes (CV) of buffer A. Ni-NTA purification fractions containing the target protein were pooled and loaded onto the Mono Q column at a flow rate of 1 mL/min. The column was washed with 5 CV of 83% buffer A and 17% buffer B to remove any unbound proteins. Bound proteins were eluted with a linearly increasing NaCl gradient. Proteins with a lower surface charge elute first. The elution of any proteins was monitored by UV absorbance at 280 nm. Peak fractions from the chromatogram were analysed by SDS-PAGE.

### 2.2.12 Size exclusion chromatography

Size exclusion chromatography (SEC or gel filtration, GF) is used to separate molecules by their hydrodynamic radii i.e. a combination of their size and shapes. Molecules pass through a matrix inside a glass column (Kazakevich and Lobrutto, 2006) without physically binding to the matrix. Separation is hence not affected by the buffer composition. SEC provides information on the oligomerisation state of a protein or a protein mixture (Fekete et al., 2014) and may also be used to exchange the buffer for down-stream experiments as the smaller buffer compounds will be separated from the larger protein (Bourven et al., 2015). In SEC, larger molecules elute first, as their accessible volume is smaller than for smaller molecules, which enter the matrix pores (Kazakevich and Lobrutto, 2006). Here, SEC served the purpose of separating ThiL and ThrB from other proteins, to exchange the buffer for crystallisation experiments, and to determine the oligomerisation state.

The SEC was run in a Superdex 200 10/300 GL column connected on the ÄKTAbasic 900. The column was equilibrated with 3 CV of crystallisation buffer at a flow rate of 0.5 mL/min. AXC fractions containing protein were pooled, concentrated to 8 mg/mL and loaded onto the column. Proteins were eluted with 1.5 CV, collected in 1.5 mL fractions. Eluting proteins were monitored by UV absorbance at 280 nm. Peak fractions from the resulting chromatogram were analysed by SDS-PAGE for purity of ThiL and ThrB proteins.

### 2.2.13 Functional analysis with thiamine-phosphate kinase

ThiL catalyses the transfer of a phosphate group from ATP to thiamine monophosphate (thiamine phosphate, TMP) to generate thiamine diphosphate (TDP) and ADP (Figure 2.1).



**Figure 2.1: The phosphorylation reaction catalysed by ThiL.** ThiL phosphorylates TMP to TDP.

To quantify the catalytic activity (phosphate transfer) of ThiL, ADP production was monitored by high pressure liquid chromatography (HPLC) and detection at 220 nm. The ThiL assay reaction mixture contained 10 mM Tris-HCl pH 8.0, 5 mM MgCl<sub>2</sub>, 1 mM ATP, 100 mM KCl, 10 mM TMP and 2 μM ThiL in a final volume of 100 μL. The negative control

involved replacing the enzyme by distilled water. Reaction mixtures were incubated at 37°C for 5 h before adding 10 mM (w/v) EDTA, a chelating agent which binds the catalytic  $Mg^{2+}$  of ThiL stopping the reaction.

### **Analysis of assay reaction component by HPLC**

HPLC is a technique that uses liquids under high pressure to separate constituent molecules from a small sample volume. The 3 to 5  $\mu m$  diameter and the properties of the column matrix allow very similar molecules to be separated with high efficiency (Horie et al., 2012). Molecules are detected through either spectroscopic, refractive, or fluorescence detection techniques (Swartz, 2010). Here, the reaction mixture was analysed using a Hypersil GOLD column (250 X 4.6 mm, 5  $\mu m$  particle size connected to a HPLC system (Ultimate 3000). The column which separates molecules based on their absorptive forces, was equilibrated with the mobile phase (0.1 M  $K_2PO_4$ , pH 6.6) at a flow rate of 1 mL/min. Twenty  $\mu L$  of the reaction mixture was loaded for each run to quantify ADP production.

#### **2.2.14 Functional analysis with homoserine kinase**

ThrB catalyses the phosphorylation of L-homoserine to O-phosphohomoserine with ATP as the phosphate donor (Figure 2.2). The assay reaction mixture contained 50 mM HEPES pH 7.0, 1 mM  $MgCl_2$ , 1 mM ATP, 450 mM KCl, 10 mM L-homoserine and 4  $\mu M$  ThrB in a final volume of 100  $\mu L$ . Incubation and analysis of assay products by HPLC was done as with ThiL.



**Figure 2.2: Phosphorylation reaction catalysed by ThrB.** ThrB catalyses the phosphorylation of L-homoserine to O-phosphohomoserine.

#### **2.2.15 Protein crystallization – finding lead conditions**

Crystallisation is affected by a number of challenges ranging from predicting the right temperature, pH, nature and concentration of precipitant, purity and stability of the protein of interest as well as the technique used (Mcperson, 2004). All these factors can affect the size and quality of crystals required for better X-ray diffraction. To overcome



some of these challenges, finding lead conditions is always a good starting point. Optimisation of the lead conditions can then provide better crystals for X-ray diffraction. Different techniques can be used to crystallise proteins, including hanging drop or sitting drop (Benvenuti and Mangani, 2007).

Here, crystallisation trials were set up for ThiL and ThrB using both sitting- and hanging-drop, vapour-diffusion techniques. A Mosquito nanolitre crystallisation robot was used to set up sitting drop crystallisation experiments in a 96-well Greiner bio-one microplate. To cover as broad a set of parameters as possible to identify lead crystallization conditions, a sparse-matrix approach as provided by the commercial crystallisation screens listed in Table 2.1 were employed. Seventy  $\mu\text{L}$  of each screening reagent was transferred to a specific reservoir of the crystallisation plate and the latter placed on the tray of the Mosquito robot. A 5  $\mu\text{L}$  volume of concentrated ThiL in 5 mM NaCl, 1 mM MgCl, 1 mM DTT and 5 mM Tris pH 7.0 with or without the substrates (TMP), inhibitor (AMP-PnP) and product (ADP) was provided. The Mosquito, operating to a defined protocol, independently transferred 200 nL of the reservoir solutions and 200 nL of the protein solution to the sitting-drop well and allowed the two solutions to mix. The plate was sealed with clear transparent tape and the wells were immediately checked using Keyence Leica DFC320 digital microscope to ensure mixing of drops in each well. The plate was stored at 18°C, periodically examined under a microscope, and changes such as precipitation and nucleation noted. The same setup was used for ThrB in 30 mM NaCl, 4 mM MgCl<sub>2</sub>, 1 mM DTT and 50 mM HEPES pH 7.5

#### **2.2.16 Optimisation of crystallisation conditions for thiamine-phosphate kinase**

Lead crystallization conditions mostly need to be optimised to produce optimal protein crystals for X-ray diffraction. By slowing the crystallization process both crystal size and quality can be improved (McPherson and Cudney, 2014). Conditions were optimised by varying the concentration of the individual components of the lead conditions in hanging drop mode. Each reservoir solution was prepared from stock solutions in one of 24 wells of a Linbro crystallization plate. A sample of 2  $\mu\text{L}$  of each reservoir solution was placed onto a cover slip and 2  $\mu\text{L}$  of the protein solution was added. The cover slip was then inverted over the reservoir solution, the rim of which had been covered with silicone

grease to insulate each individual experiment. The plate was stored at the required temperature. The plate was repeatedly analysed visually under Zeiss discover microscope for noticeably changes including protein precipitation and crystal formation. Optimisation was repeated at different temperatures and different pHs.

To improve the size and quality of crystals, seeding was used. A seed provides a template for which further crystals can grow. Seeding allows to control the nucleation and some features of the resulting crystal because it will inherit many of the features of the seeds from which it originated. Seeding can be done using macro (where the seed can be seen) or micro (where only invisible small splitters are used as seeds)-seed. For this study, micro-seeds and different times of seeding were used.

To prepare protein/substrate, protein/inhibitor or protein/product complexes, substrates, inhibitors and products were added to the protein solution prior to setting up crystallization experiments to achieve final concentrations of 0.4 to 1 mM. Co-crystallisation experiments included either TMP (substrate), AMP-PnP (inhibitor) or ADP (product) alone or the combinations TMP/AMP-PnP (substrate and substrate-like inhibitor) or ADP/TDP (products).

To prepare protein crystals for data collection at 100 K they need to be protected against the process of water freezing. This is done by adding cryo-protective compounds such as PEG 400, glycerol and MPD which allow a clear glass-like state when cooled to below 0°C. Here, sufficient PEG 400 was added to a sample of the reservoir solution to achieve a final concentration of 30% (v/v). Crystals were transferred to the cryo-solution for a few seconds before being plunged into liquid nitrogen. X-ray diffraction data were collected at the European Synchrotron Radiation Facility (ESRF) in Grenoble, France.

#### **2.2.17 Optimisation of crystallisation conditions for homoserine kinase**

The same setup as that of ThiL was employed for optimisation with ThrB. A final protein concentration of 15 mg/mL in 30 mM NaCl, 4 mM MgCl<sub>2</sub>, 1 mM DTT and 50 mM HEPES pH 7.5 was used. Co-crystallisation experiments involving the substrate L-homoserine, the substrate analogue inhibitor AMP-PnP, and the product ADP at concentrations between 1 and 4 mM were also set up. Optimisation started from initial conditions (15% (w/v) PEG 10 000, 0.2 M MgCl<sub>2</sub>, 0.1 M MES pH 6.8) obtained during screening.

Crystallization conditions were optimised by changing the temperatures, the pH and by adjusting the concentration of the reservoir components. For X-ray diffraction, crystals were cryoprotected using 30% (v/v) PEG 400. Diffraction experiments were also attempted at the ESRF.

### **Data collection and structure determination of thiamine-phosphate kinase**

Cryo-protected crystals of ThiL and ThrB were sent to the ESRF in Grenoble, France at a temperature of 100 K. Here crystals were analysed and diffraction data collected automatically on the beamline MASSIF-1/ID30A-1 (Hartley et al., 2000a, b). The crystal structure for ThiL was solved using molecular replacement (PHENIX) using ThiL from *Aquifex aeolicus* (90% coverage, 30% identity) and *Acinetobacter baumannii* (78% coverage, 33% identity) as potential models. ThiL from *Aquifex aeolicus* was finally chosen as the best model for molecular replacement (MR) due to higher sequence coverage (90%). After first rounds of MR failed, the model was modified using sculptor (PHENIX) to remove any extended loops. PHENIX autobuild and refinement routines were used to build a model from an initially uninterpretable electron density maps. The model was further extended and improved manually using WinCoot and PHENIX refine routines. The final structure was analysed using PyMol.

## 3 Results

### 3.1 Restriction digest of ThrB-pET20b and ThiL-pET28a plasmids

The plasmids ThrB-pET20b and ThiL-pET280 were restriction digested using XhoI and NdeI to confirm the sizes of *thrB* and *thiL* genes insert in their respective plasmids.

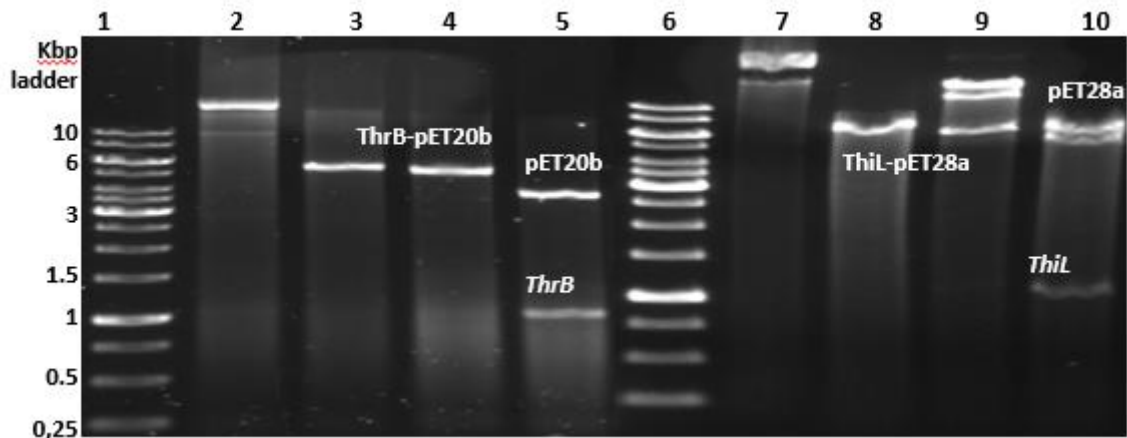


**Figure 3.1: 1% agarose gel of ThrB-pET20b and ThiL-pET28a restriction digest.**

Lane 1: 1 kbp ladder; 2: undigested ThrB-pET20b; 3: single digest with XhoI; 4: single digest with NdeI; 5: double digest with XhoI and NdeI; 6: 1 kbp ladder; 7: undigested ThiL-pET28a; 8: single digest with XhoI; 9: single digest with NdeI; 10: double digest with XhoI and NdeI.

Single restriction digest of ThrB-pET20b with either XhoI or NdeI resulted in a single band of size 4538 bp (figure 3.1, lane 3 and 4) corresponding to the linearised full-length plasmid. Digesting the plasmid with both enzymes simultaneously produced two bands of 3700 and 800 bp (figure 3.1, lane 5) corresponding to the original vector plus the insert (gene of interest). Similarly, single digestion of ThiL-pET28a with XhoI resulted in a single band of 6300 bp – the size of the linearized vector (figure 3.1, lane 8), while NdeI digest produced two additional bands above the expected 6300 bp band (figure 3.1, lane 9). A double digest of ThiL-pET28a with both XhoI and NdeI produced two bands of 5300 (plasmid) and 900 bp (insert), lane 10.

### 3.2 Protein production and purification

#### 3.2.1 Production test for His<sub>6</sub>-thiamine-phosphate kinase

*E. coli* BL21 (DES) cells containing ThiL-pET28a plasmid were used for protein production.

Protein production was optimised with respect to temperature and IPTG concentration to maximise yield and solubility of the His<sub>6</sub>-ThiL (ThiL) fusion protein. Production was monitored at 37, 28, and 22°C while IPTG concentrations of 0.1, 0.15 and 0.2 mM were investigated with production continuing overnight at 200 rpm.

Protein bands of size 36 kDa, corresponding to ThiL, were observed for all IPTG concentrations and temperatures (figure 3.2). Thicker bands corresponding to larger amounts of ThiL were found after inducing with 0.1 mM IPTG as compared to 0.15 and 0.2 mM – while maintaining the same temperatures. In addition, more ThiL is invariably observed in the insoluble (figure 3.2 lanes 4, 7 and 10) as compared to the soluble fraction (figure 3.2, lanes 5, 8 and 11) for all investigated temperatures and IPTG concentrations. More soluble ThiL was obtained at 22°C (figure 3.2 C: lanes 5, 8 and 11) compared to 28°C and 37°C - irrespective of the IPTG concentration.

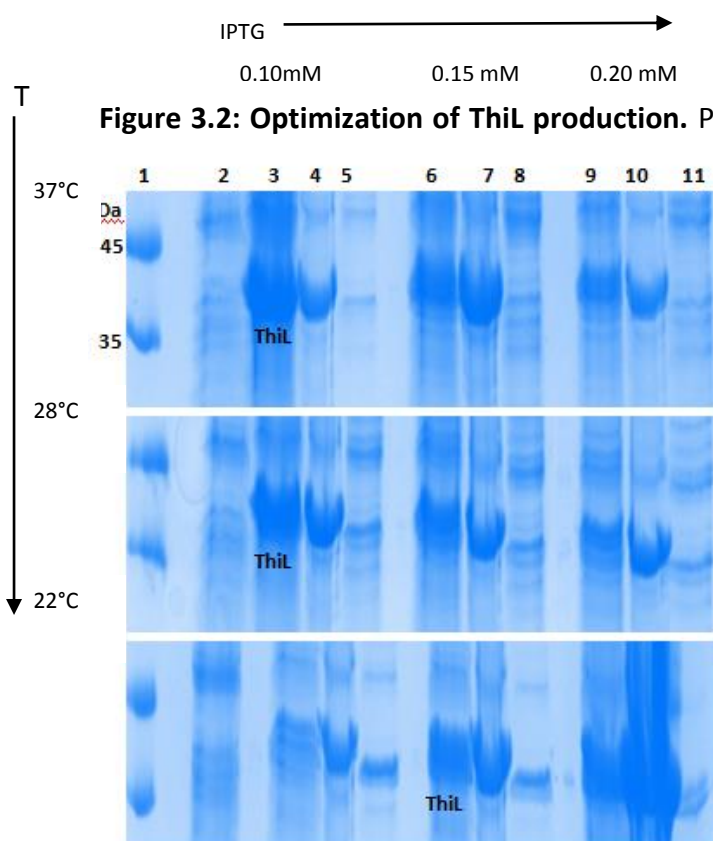


**Figure 3.2: Optimization of ThiL production.** Protein production for various conditions

was investigated by SDS-PAGE.

Lane 1: Unstained protein molecular weight marker; lane 2: samples without induction; lanes 3 to 5: induction with 0.1 mM IPTG: whole cell, insoluble and soluble fractions respectively; lanes 6 to 8: induction with 0.15 mM IPTG: whole cell, insoluble and soluble fraction; lanes 9 to 11: induction with 0.2 mM IPTG: whole cell, insoluble and soluble fractions.

**A:** Production at 37°C, **B:** 28°C, **C:** 22°C.

**C:** All inductions were for 6 h.

### 3.2.2 Production and purification of thiamine-phosphate kinase

ThiL production was scaled up to a 4 L culture to purify ThiL for crystallisation and functional analysis. Protein production and purification by affinity chromatography was performed as described in sections 2.2.4 and 2.2.7.

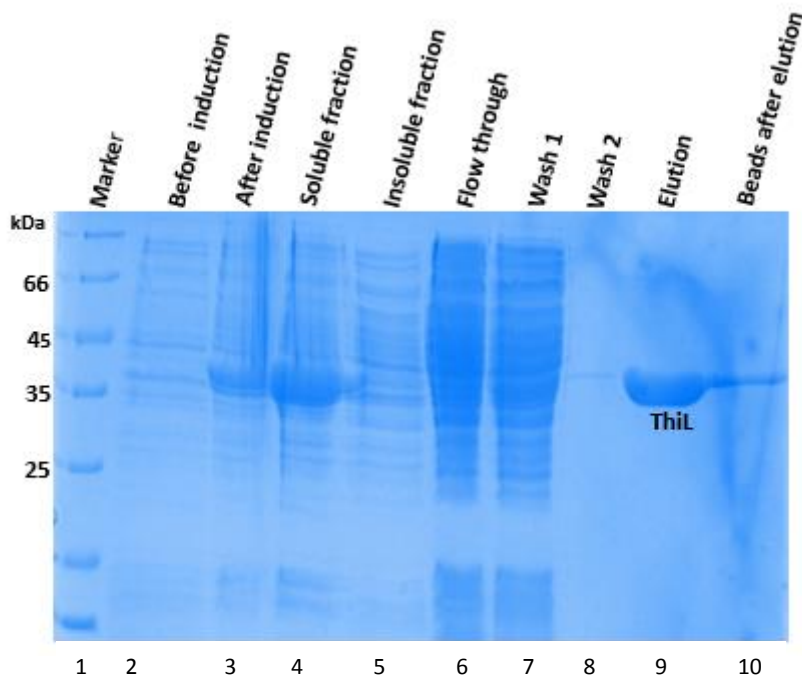


**Figure 3.3: 15% SDS-PAGE of ThiL after production and purification** Lane 1: Molecular weight marker; lane 2: Sample before induction; lane 3: Sample after induction; lanes 4 and 5: Soluble and insoluble fractions; lane 6: Unbound protein fraction; lanes 7 and 8: Unspecifically bound fractions 1 and 2 eluted with 20 mL and 500 mL wash buffer respectively; lane 9: Imidazole elution fraction; lane 10: Beads after elution. A band corresponding to ThiL (36 kDa) is observed in lanes 3, 4, 8, 9, and 10 but not in lanes 2, 6, and 7.

After induction a band of 36 kDa appeared in the soluble fraction (figure 3.3, lanes 3 and 4). As this matches the expected size of ThiL, purification was attempted. A small amount of ThiL did not bind to the beads and was lost during elution of unbound proteins (“flow through”, figure 3.3, lane 6) and during removal of non-specifically bound proteins (“wash fraction”, figure 3.3, lanes 7 and 8). ThiL was efficiently eluted with reduced imidazole buffer yielding largely pure protein (figure 3.3, lane 9).

### 3.2.3 Anion exchange chromatography with thiamine-phosphate kinase

ThiL was further purified by anion exchange chromatography (AXC). Elution of bound molecules using an increasing NaCl gradient yielded a single peak with minor shoulders

both to the left and the right of the main peak (figure 3.4, blue curve). SDS-PAGE analysis of the peak fractions revealed a 36 kDa band (ThiL) for each fraction (figure 3.4, inserted SDS-PAGE). Other protein bands were observed in the fractions corresponding to the shoulder preceding the main peak indicating that AXC had successfully removed a minor contaminant.

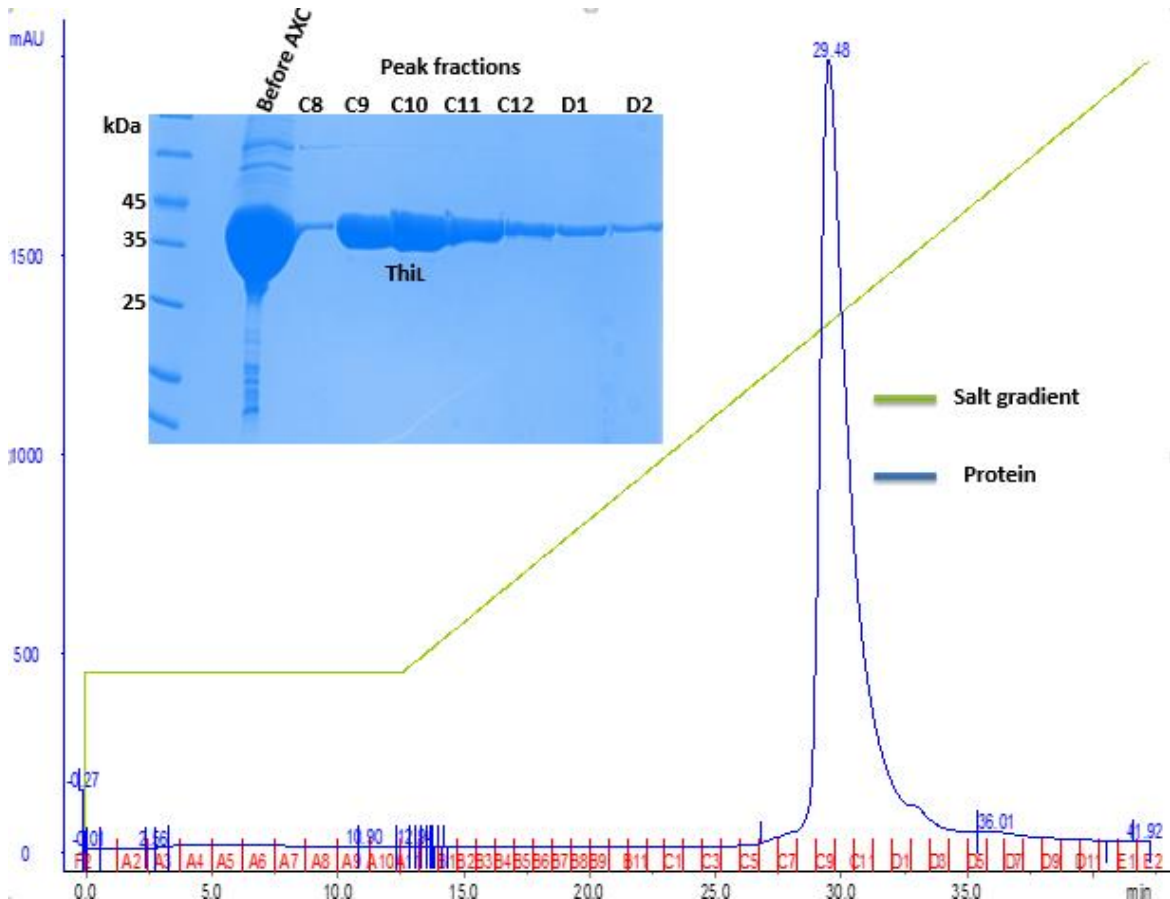


**Figure 3.4: Purification of ThiL by Anion Exchange Chromatography.** A single peak with minor shoulders both to the left and the right of the main peak is observed on the chromatogram. The sample before AXC (shown on inserted SDS-PAGE) still contain other impurities, most of which were removed during AXC. The chromatogram peak fractions contain mostly ThiL which is purer than sample before AXC.

### 3.2.4 Size exclusion chromatography with thiamine-phosphate kinase

The protein was further purified and the buffer simultaneously replaced by size exclusion chromatography (SEC) to reduce the complexity of the buffer. A single peak is observed in the chromatogram (figure 3.5). SDS-PAGE analysis of the peak fractions revealed a 36 kDa band (figure 3.5, inserted SDS-PAGE) corresponding to the size of ThiL. A contaminant

protein (top band, figure 3.5, inserted SDS-PAGE) present in the sample before SEC was absent after SEC indicating its successful removal.

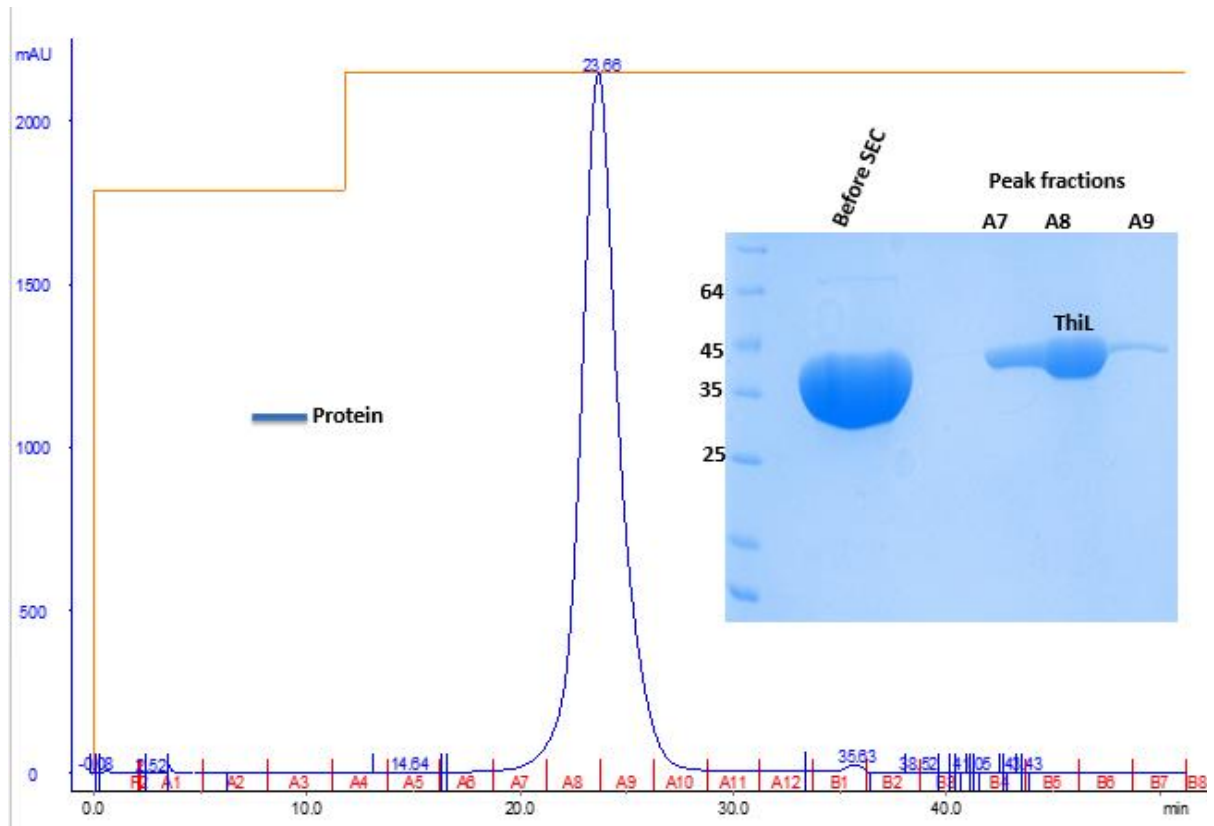


**Figure 3.5: Chromatogram of SEC with ThiL.** A: A single peak is observed after SEC, and the peak fraction A7-A9 contained only ThiL as revealed by the inserted SDS-PAGE. The sample before SEC contained a top band which was further separated from ThiL.

### Purification table for thiamine-phosphate kinase

The total amount of ThiL recovered after each purification step was recorded to analyse the effectiveness of the methodology. Table 3.1 shows that a significant amount of protein was lost during AXC compared to Ni-NTA affinity purification and SEC.

**Table 3.1: Purification table for ThiL**

Weight of pellet/ L culture (g)	Total soluble protein (mg)	Total ThiL after Ni-NTA purification (mg)	Total ThiL after AXC (mg)	Total ThiL after SEC (mg)
11.4	30	6	3.5	2.6



### 3.2.5 Production test for homoserine kinase

For the production test with ThrB, the same procedure as that of ThiL was applied (section 3.2.1). Protein bands of size 33 kDa, corresponding to ThrB, were observed in the insoluble fractions, after induction and in the soluble fractions for all temperatures and IPTG concentrations tested (figure 3.6). The ThrB band is most intense when produced at 37°C compared to the other temperatures.

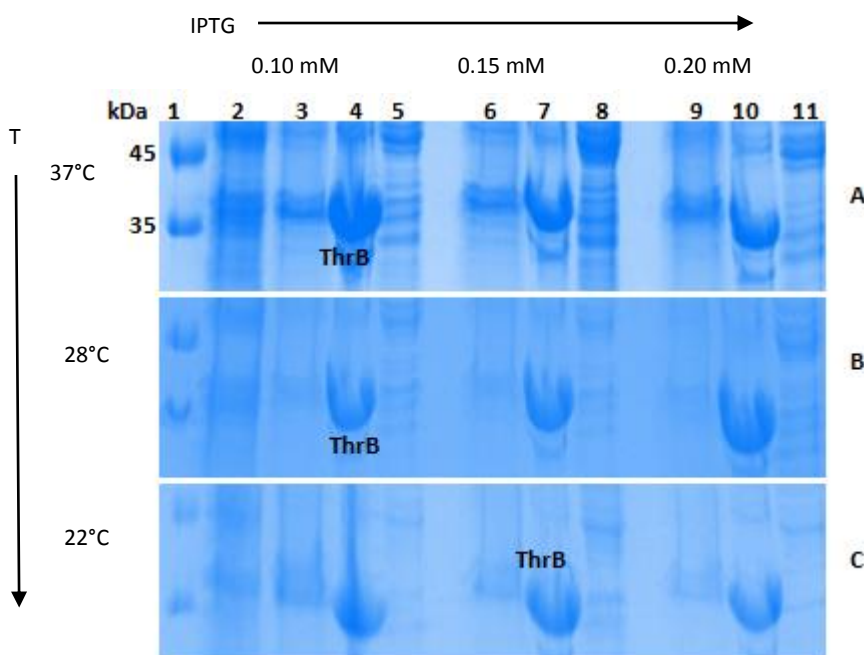


**Figure 3.6: Optimization of ThrB production analysed by SDS-PAGE.** Lane 1: Unstained protein molecular weight marker; lanes 2: no induction; lanes 3 to 5: Induction with 0.1 mM IPTG: whole cell, insoluble and soluble fraction, respectively; lanes 6 to 8: Induction with 0.15 mM IPTG: whole cell, insoluble and soluble fractions; lanes 9 to 11: Induction with 0.2 mM IPTG: whole cell, soluble and soluble fractions. **A:** Production at 37°C, **B:** 28°C, **C:** 22°C. All inductions were done for 6 h.

The larger amount of ThrB is observed in the insoluble fractions at all the temperatures and IPTG concentrations tested (figure 3.6), with small amounts of soluble ThrB observed at 22°C for all IPTG concentrations (figure 3.6). To quantify the amount of ThrB in the soluble fraction, the fraction was added to Ni-NTA resin, nonspecifically bound proteins removed, ThrB eluted with imidazole buffer and fractions analysed by SDS-PAGE. The soluble fraction at 22°C contained the highest amount of ThrB, independently of the IPTG concentration (results not shown). ThrB was produced from 6 L of medium at 22°C with 0.1 mM IPTG and aeration at 170-190 rpm.

### 3.2.6 Production and purification of homoserine kinase

ThrB was produced and purified analogously to ThiL (section 3.2.2). SDS-PAGE analysis revealed a 33 kDa band (ThrB) after induction with most protein insoluble rather than soluble (figure 3.7, lanes 3, 4 and 5).

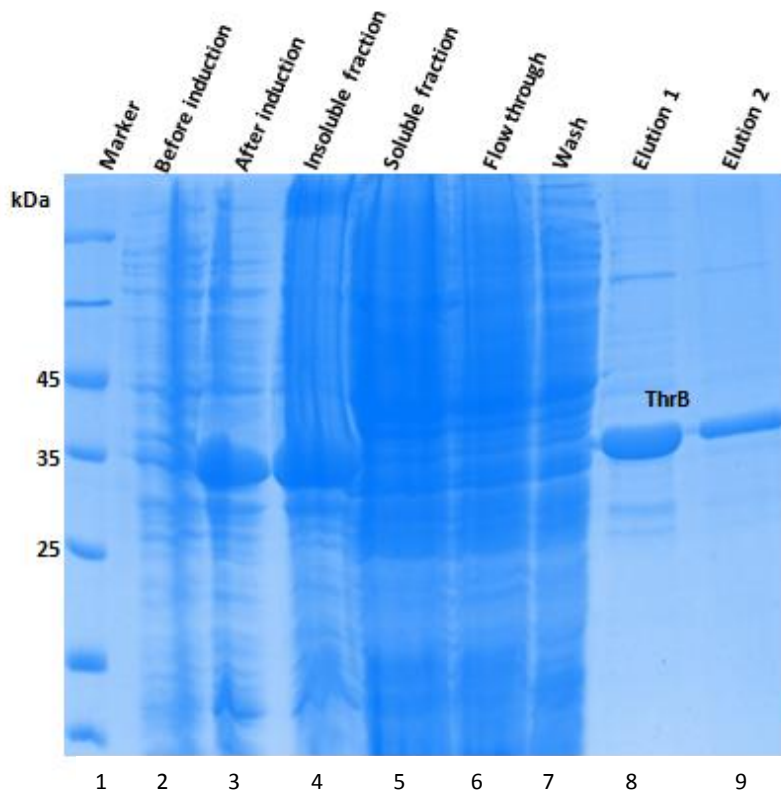


**Figure 3.7: 15% SDS-PAGE of ThrB production and purification.** Lane 1: Molecular weight marker; lanes 2 and 3: Before and after induction; lanes 4 and 5: Insoluble and soluble fractions; lane 6: unbound fraction; lane 7: non-specifically bound fraction (“wash”); lanes 8 and 9: Imidazole elutions 1 and 2.

Bands at 33 kDa corresponding ThrB is observed in lanes 3, 4, 8 and 9. Only small amount of the same band is observed in lane 5.

After coupling the soluble fraction to Ni-NTA resin and washing, no ThrB band was observed in the flow through and washes (figure 3.7, lanes 6 and 7). ThrB was, however, successfully eluted from the resin (figure 3.7, lanes 8 and 9) – though contaminated by other protein bands.

### 3.2.7 Anion exchange chromatography with homoserine kinase

ThrB was further purified by anion exchange chromatography (AXC) as described in 2.2.11. The chromatogram indicated a single peak with minor shoulders both before and

after the main peak (figure 3.8). SDS-PAGE analysis of the peak fractions revealed a 33 kDa band (ThrB) in addition to other protein bands (figure 3.8, SDS-PAGE insert).

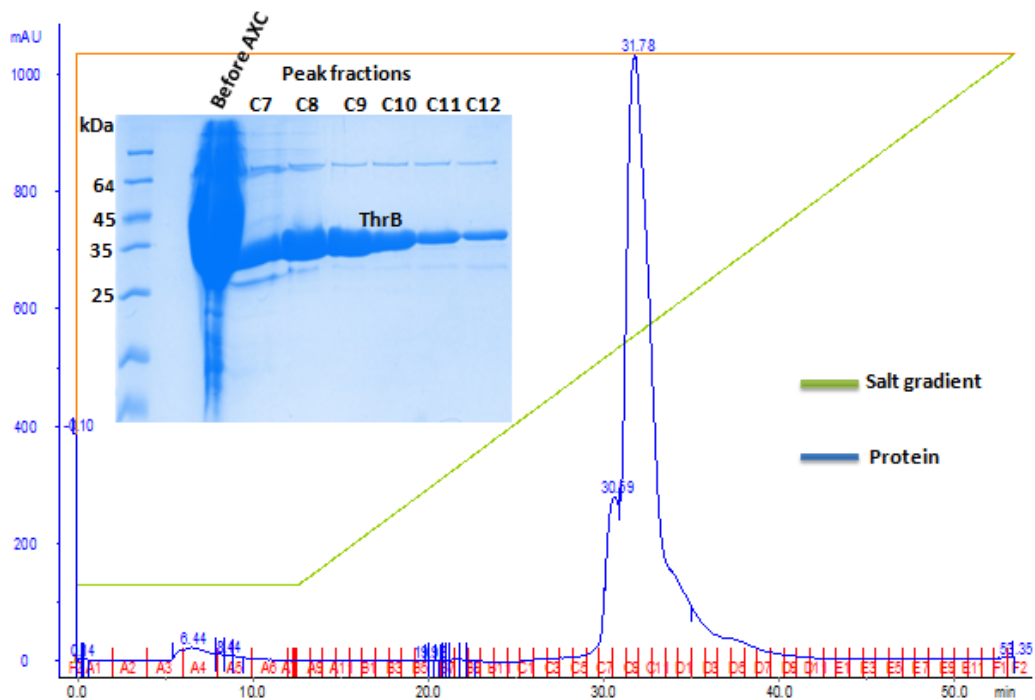


**Figure 3.8: Chromatogram for ThrB AXC.** The chromatogram displays a single peak with minor shoulders on either side of the main peak. Insert: SDS-PAGE analysis of peak fractions C7 to 12 indicates that these fractions mostly contained ThrB (33 kDa) with some additional protein bands still present as well. Most contaminating proteins observed in pre-AXC sample had been removed by ion-exchange chromatography.

### 3.2.8 Size exclusion chromatography with homoserine kinase

SEC as described in section 2.2.12 was used to further purify ThrB. Two peaks (1 and 2) were observed on the chromatogram (figure 3.9). SDS-PAGE analysis of the peaks fractions revealed that peak 1 contained proteins larger in size than ThrB while peak 2 contained ThrB only. Fractions C3 and C4 of peak 2 contained high purity ThrB (figure 3.9 insert). They were pooled and used for downstream experiments.

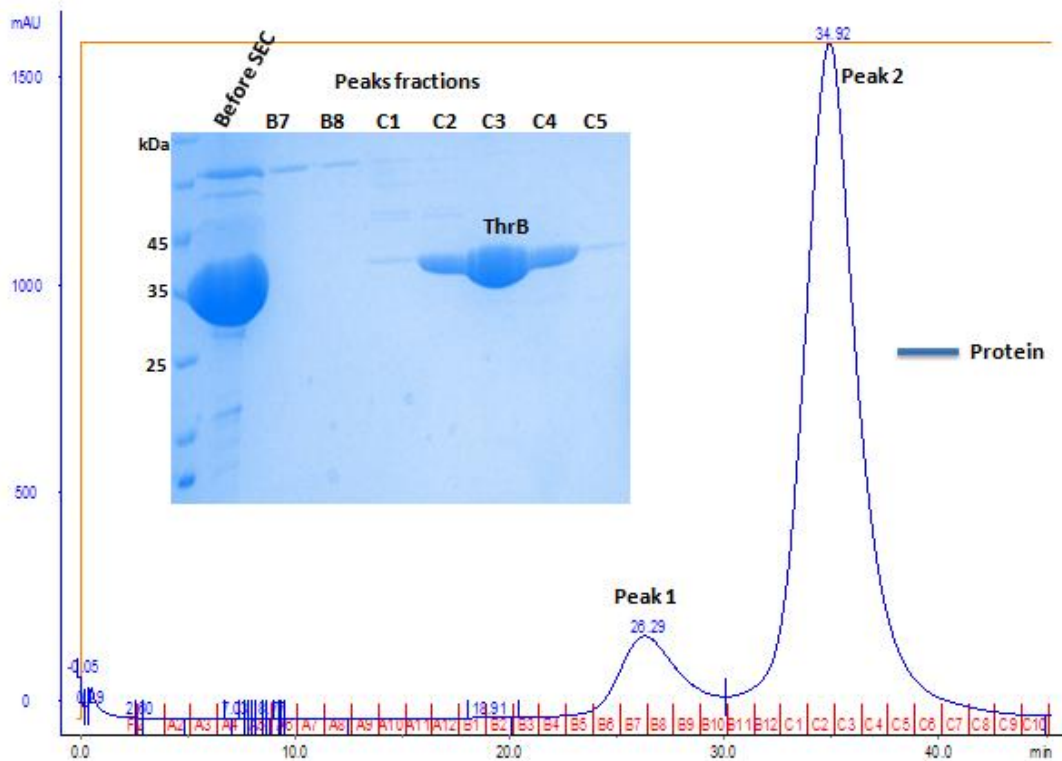


**Figure 3.9: SEC chromatogram for ThrB.** Two distinct peaks are observed. Insert: SDS-PAGE analysis of the corresponding fractions indicates that proteins constituting peak 1 were larger in size than ThrB. The latter predominated in peak 2. Fractions C3 and C4 were of highest purity.

### Purification table for homoserine kinase

A purification table for ThrB indicates that ThrB was mostly lost during AXC (table 3.2).

**Table 3.2: Purification table for ThrB**

Total cell mass (mg)	Total soluble protein (mg)	ThrB after Ni-NTA purification (mg)	ThrB after AXC (mg)	ThrB after SEC (mg)
13 200	15	1.2	0.6	0.4

### 3.3 Functional analysis with thiamine-phosphate kinase

Active ThiL should phosphorylate TMP to TDP and using ATP as the phosphate donor (section 2.2.13). Using HPLC, the reaction components were analysed to identify and quantify reactants and products. The retention times between sample injection and the

tip of the corresponding peaks were used to identify individual molecules. The amount of each component present was estimated from the area under the peak.

### 3.3.1 Analysis of standards

Molecular standards were used to obtain fingerprint retention times for all relevant molecules involved in the enzymatic reaction of ThrB. ATP, ADP and TMP were each run separately to unambiguously determine their retention times.

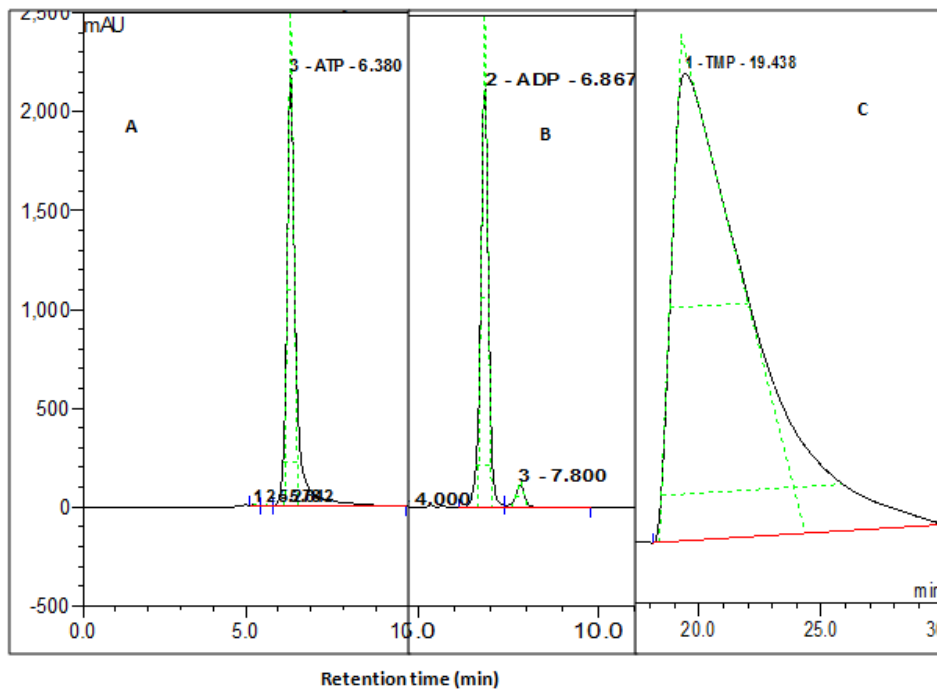


**Figure 3.10: HPLC chromatograms for individual standards recorded at 210 nm. A:** ATP retention time was 6.38 min; **B:** ADP: retention time is 6.87 min. A second, smaller peak 3 at 7.80 min was also observed but may be due to a contamination; **C:** TMP retention time is 19.44 min.

For ATP a single peak with retention time of 6.38 min was observed (figure 3.10 A), whereas the analysis of ADP produced a taller and a shorter peak with retention times of 6.87 and 7.80 min (figure 3.10 B), though the latter presumably is due to a contamination in the standard sample. For TMP a single peak with a retention time of 19.44 min was observed (figure 3.10 C).

### 3.3.2 Analysis of thiamine-phosphate kinase assay component

The reaction mixture from each ThiL assay was analysed by HPLC for the production of ADP as one of the products. Both standards and the assay mixture were analysed on a single HPLC batch run allowing standards to identify corresponding components in the

assay mix. The chromatogram confirmed ATP and TMP (reactant) peaks for the negative control reaction (no ThrB, figure 3.11 A). The assay run produced five peaks corresponding to ATP, ADP, TDP and TMP based on the retention times of the standards (figure 3.11 B).

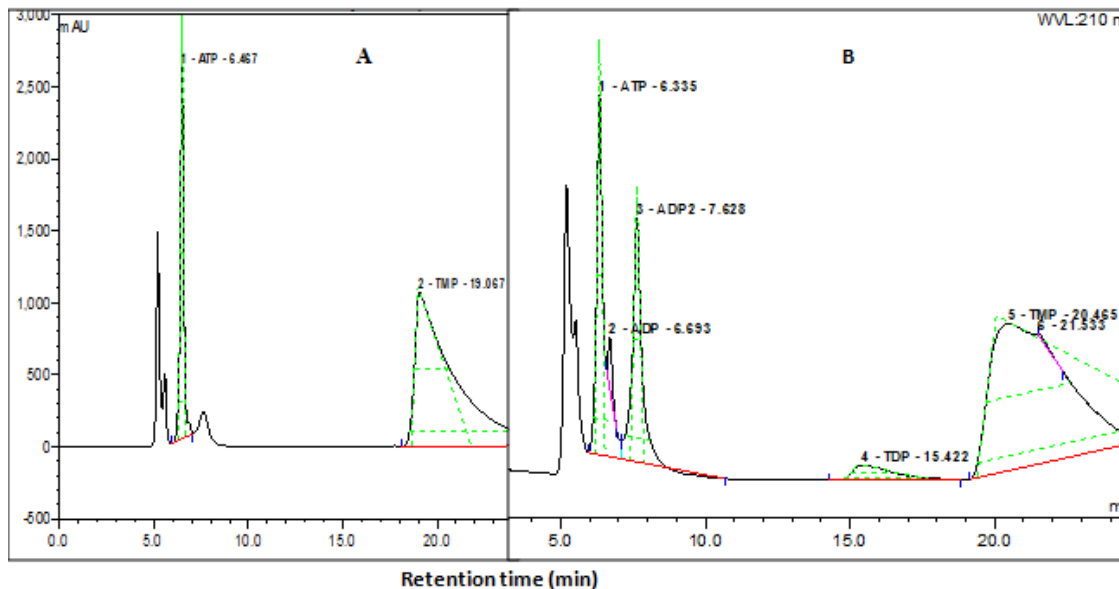


**Figure 3.11: HPLC chromatogram for a ThiL reaction assay.**

**A:** Negative control: 1 mM ATP, 10 mM TMP, 10 mM Tris pH 8.0, 100 mM KCl, 5 mM MgCl<sub>2</sub>, no ThiL.

**B:** Experimental run with components as listed in **A** plus 5 μM ThiL. Only ATP and TMP peaks were observed in the negative control, whereas the experimental produced peaks corresponding to ADP and TDP in addition to those of ATP and TMP. Relevant peaks are marked in green.

### 3.3.3 Functional analysis with homoserine kinase

ThrB catalyses the transfer of phosphate group from ATP to homoserine to produce ADP and O-phosphohomoserine (section 2.2.14). The activity assay and detection of assay component was performed as outlined in section 2.2.13. The standards used in identifying the molecules of interest in the assay reaction included ATP and ADP as analysed in section 3.3.1.

### 3.3.4 Analysis of homoserine kinase assay component

The assay reaction incubated for 4 h was analysed by HPLC (section 2.2.14) for ADP production. While the negative control resulted in ATP peaks only (figure 3.12 A), the

experimental run additionally displayed a peak for ADP (figure 3.12 B). Additional peaks are visible but because of a lack of standards, these could not be identified.

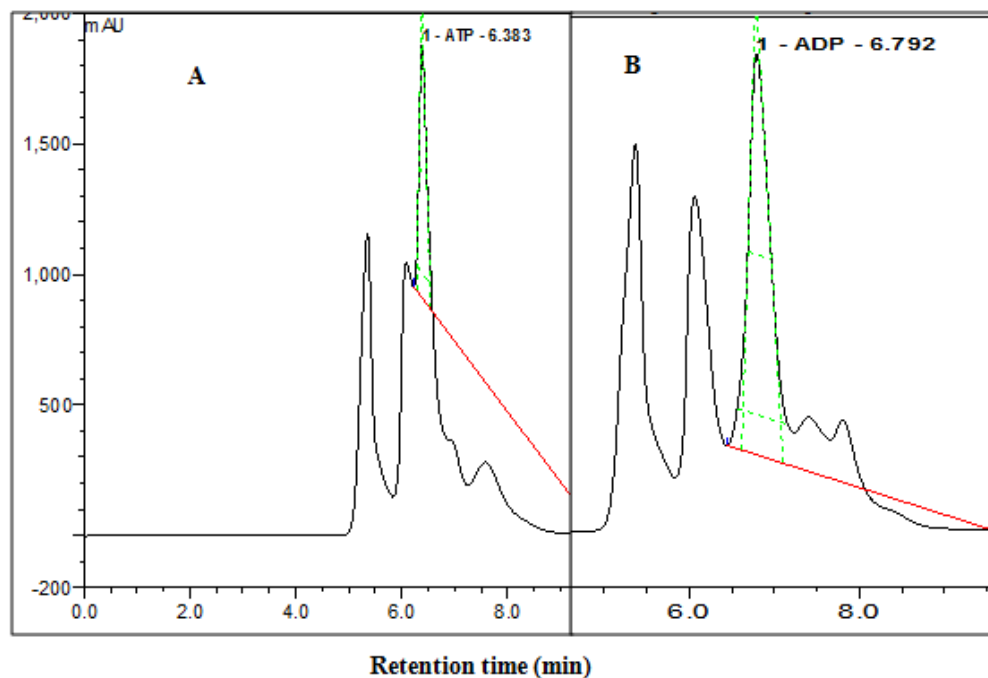


**Figure 3.12: HPLC chromatogram for ThrB assay.**

**A:** Negative control: 50 mM HEPES pH 7.0, 1 mM MgCl<sub>2</sub>, 1 mM ATP, 450 mM KCl, 10 mM homoserine.

**B:** Experimental run: components as in **A** plus 4 μM ThrB.

### 3.4 Crystallisation experiments with thiamine-phosphate kinase

Initial conditions (10% (w/v) PEG 10 000, 0.2 M MgSO<sub>4</sub>, 0.1 M sodium cacodylate pH 6.5) with 20 mg/mL ThiL in 5 mM NaCl, 1 mM MgCl, 1 mM DTT and 5 mM Tris pH 7.0 at 4°C yielded crystals in the form of needles, appearing in clusters after 2 days ( figure 3.13).

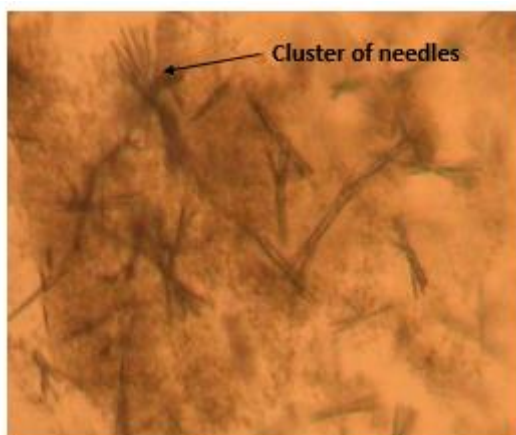


**Figure 3.13: Crystals obtained from initial sparse-matrix screen with ThiL.** Needle-shaped crystal clusters were observed, the crystals of which did not grow any further over time.

### 3.4.1 Optimisation of crystallisation conditions for thiamine-phosphate kinase

Lead ThiL crystallization conditions were optimized to improve crystal quality for X-ray diffraction and structure determination. Testing for different ThiL concentrations between 18 and 25 mg/mL yielded similar crystals implying that the protein concentration in this narrow range was not critical. Repeating the experiments at 4, 8, 16 and 22°C re-produced the crystals at 4 and 8°C after 2 days with the number, size and morphology of crystals being similar (figure 3.13).

### 3.4.2 pH optimisations

Crystals were observed at all investigated pHs (pH 4, 5, 6 and 6.9), with better crystals at pH 6.0 and 6.9 (figure 3.14). At or below pH 5.0, the protein rapidly precipitated, producing dense needle clusters (figure 3.14 A). More separated needles resulted at pH 6 and 6.9 (figure 3.14 B and C).

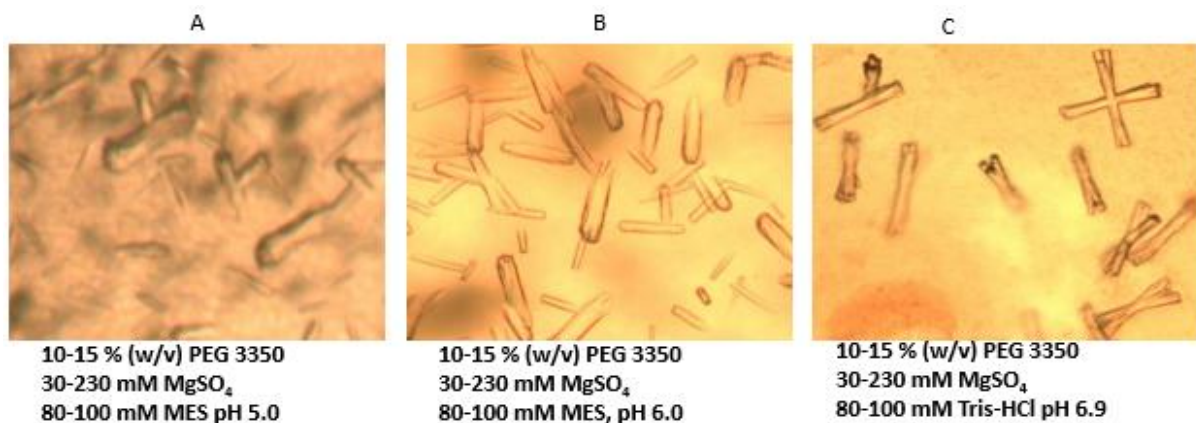


**Figure 3.14: pH optimisation for formation of ThiL crystals.** A: MES pH 5.0; B: MES pH 6.0; C: Tris-HCl pH 6.9. Thick needle clusters results at pH 5.0; crystals are more distinct at pH 6.0 and 6.9.

### 3.4.3 Precipitant and salt optimisation

Two common components of crystallization buffers are the precipitant, mostly organic molecules with different oxygen functional groups. The precipitant and salt identified in the initial screen were PEG 3350 and MgSO<sub>4</sub> respectively. Their concentration was systematically altered to try to improve the crystal quality while both the protein concentration (18 mg/mL) and the buffer systems (MES pH 6.0 and Tris-HCl pH 6.9) were kept constant.



The size and morphology of ThiL crystals were optimal at PEG 3350 concentrations of 13 to 15% (w/v) (figure 3.16A-J). Crystal optimisation with the MES pH 6.0 buffer overall proved more amenable to producing usable crystals with crystals growing in all three dimensions (figure 3.15 A, B, C and E) whereas crystals from the Tris-HCl pH 6.9 buffer resulted in elongated, needles with lateral splitting (figure 3.15 F-J).

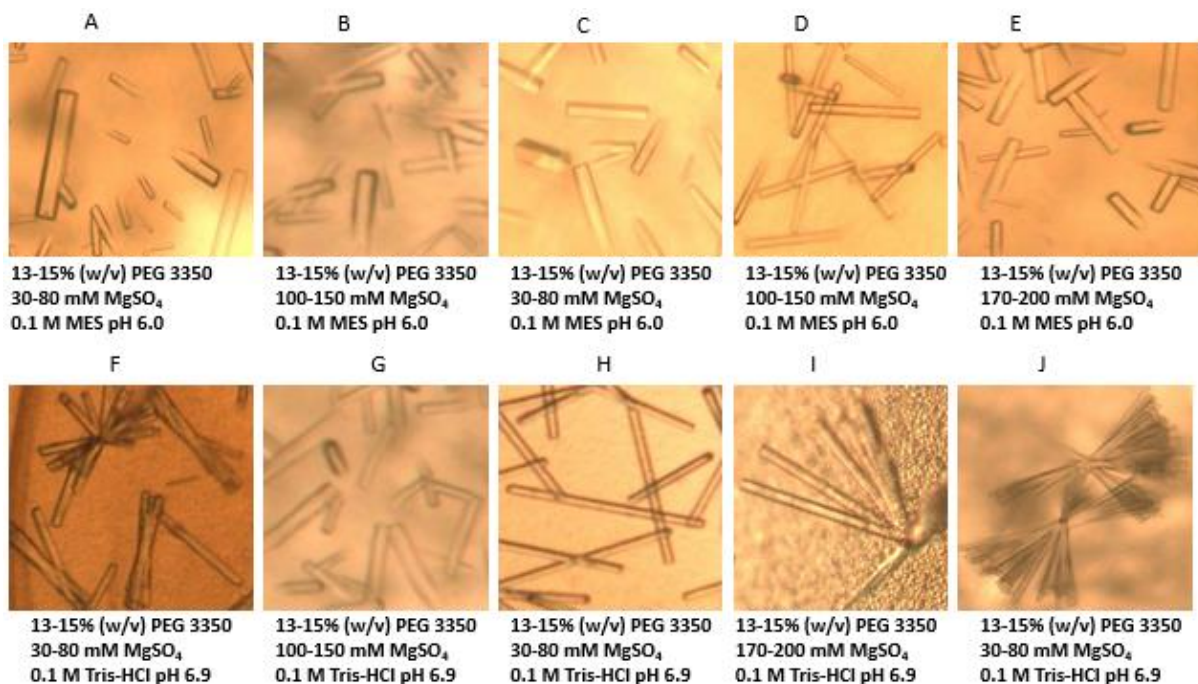
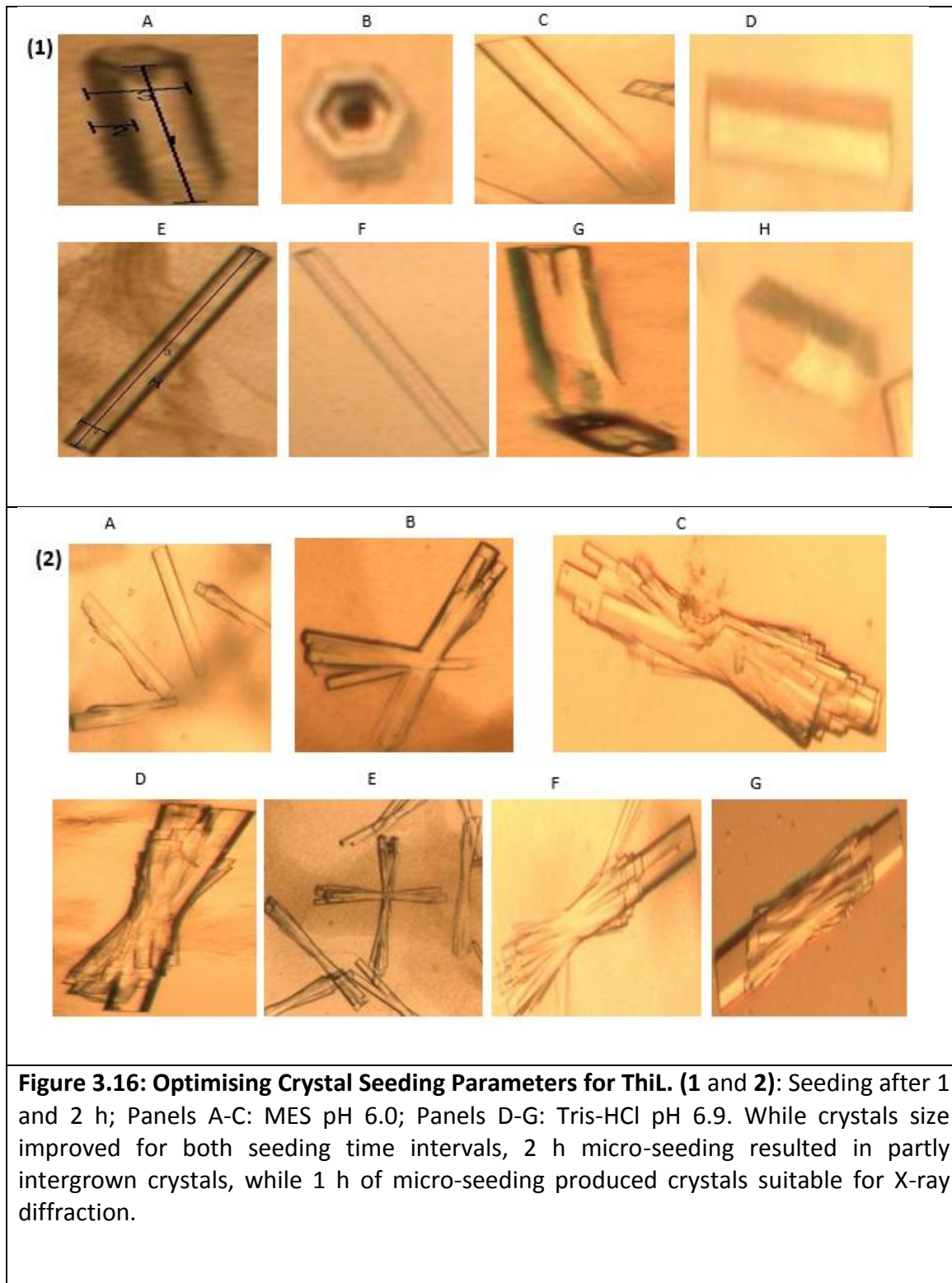


**Figure 3.15: ThiL crystals obtained by optimising precipitant and salt concentrations.** ThiL crystals obtained using different PEG 3350 and MgSO<sub>4</sub> concentrations based on either a MES pH 6.0 (A-E) or Tris-HCl pH 6.9 (F-J) buffer systems.

### 3.4.5 Optimising Crystal Seeding

Protein crystals are thought to develop from crystal nuclei, consisting of a small number of molecules arranged in a crystalline manner. Formation of such nuclei is a slow and poorly understood process. However, this uncertainty may be eliminated by adding crystal nuclei to the crystallization drop, with nuclei deriving from crystals obtained in previous rounds of crystallization. This principle was applied to ThiL crystallization through micro-seeding, which involves crushing crystals, diluting the crystal fragments and adding a small volume of this suspension to a previously pipetted crystallization drop. A number of variables may need to be optimized, including identifying the optimal time interval between experimental setup and adding the nuclei. The size of resulting crystals

was observed to benefit from a delay of 1 to 2 h between setup and seeding. Note that this was true for both pH 6.0 or 6.9 (figure 3.16, (1) and (2))



Crystal micro-seeding dramatically improved the size of ThiL crystals both for a 1 or a 2 h delay after setup, though micro-seeding after 1 h produced slightly better crystals overall

(figure 3.16). Crystals measuring around  $120 \times 90 \times 56 \mu\text{m}^3$  were sufficiently large for X-ray diffraction. Crystals were invariably hexagonal shape (figure 3.16) independent of pH.

### 3.5 X-ray diffraction, data collection and refinement of thiamine-phosphate kinase

X-ray diffraction is a prerequisite for determining the structure of a protein by X-ray crystallography. An image obtained from one of 12 ThiL crystals irradiated during a trip to the European Synchrotron Radiation Facility (ESRF) in July 2016 is typical for protein diffraction (figure 3.17). Data indexing and processing, image scaling and merging of reflections were completed by the automatic pipeline provided at the ESRF. The data collection statistics are summarised in table 3.3.

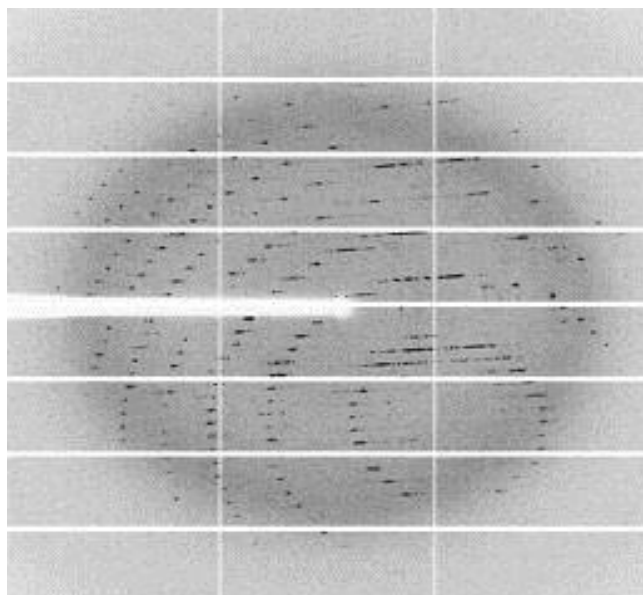


**Figure 3.17: X-ray diffraction image obtained from a ThiL crystal.**

**Table 3.3: Summary of data collection statistics for ThiL crystal**

Data collection statistics	
Beamline	MASSIF-1/ID30A-1 (ESRF)
Wavelength (Å)	0.966
Energy (KeV)	12.8
Exposure time (s)	0.1
Number of images	680
Detector distance (mm)	330.09
Resolution at edge (Å)	2.7
Resolution at corner (Å)	1.8
Number of unique reflections	15 225

### 3.5.1 Crystal structure of *Mycobacterium tuberculosis* thiamine-phosphate kinase

To determine the crystal structure of a protein, the molecular replacement technique can be used. This method may be applied if a similar structure is available. In the case of thiamine-phosphate kinase from Mtb, the structure of ThiL from *Aquifex aeolicus* (Kollewe *et al.*, 2004), PDB code 1VQV) was used as a model. It shares 33% sequence identity with MtbThiL. Density calculations indicated that one molecule occupies the asymmetric unit. Following the placement of *A. aeolicus* ThiL model structure in the unit cell using “Phenix Replace” (Mccoy *et al.*, 2007) the quality of the electron density was found to be insufficient to allow manual manipulation and improvement of the model. Instead “Phenix Rebuild” (Mccoy *et al.*, 2007), a program used for model rebuilding and completion was used to improve the model, resulting in a significantly better protein model and a dramatically improved electron density map, indicating that the structure factor phases calculated from the structural model had improved significantly.

Inspecting the electron density map for ThiL indicated that defined electron density was lacking for the N-terminal 73 and the C-terminal 12 residues – presumably due to inherent disorder in these domains. These residues correspondingly had to be excluded from the final structural model. Further rounds of manual optimization alternating with structure refinement with Refmac5 (Hao, 2004), a program designed for refinement of macromolecular structures led to the final model, the statistics for which are listed in Table 3.4.

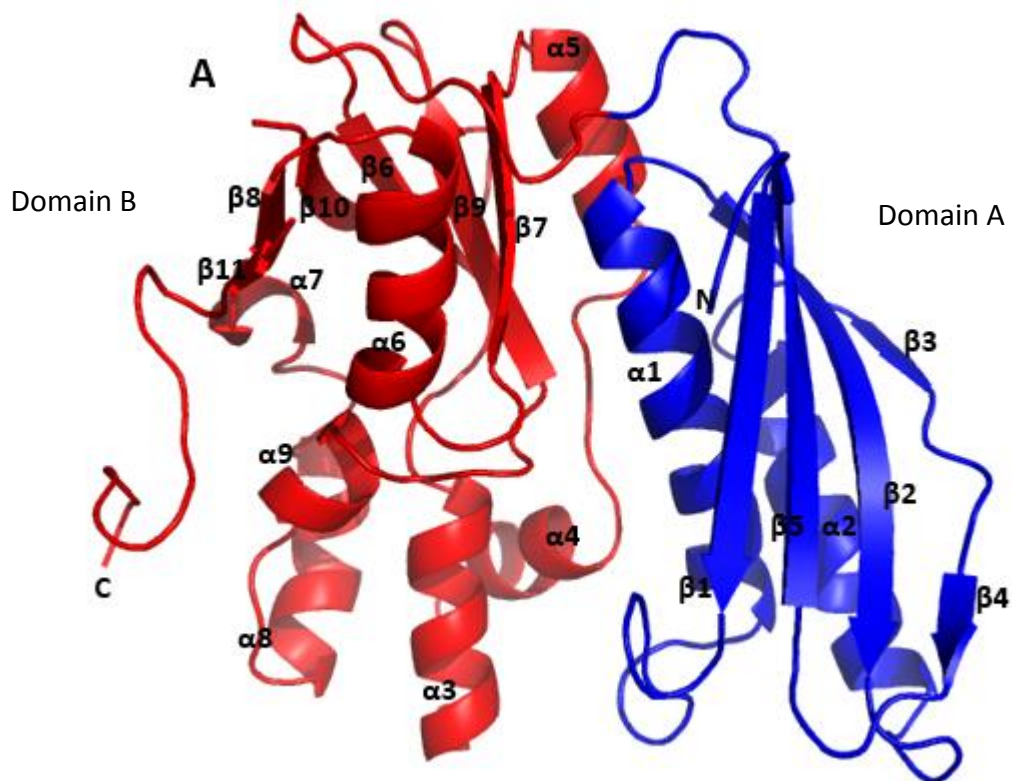
**Table 3.4: Summary of refinement statistics for ThiL crystal**

Refinement statistics	
Reflections used for refinement*	14486 (902)
Reflections used for R-free*	1440 (89)
R-work*	0.25 (0.39)
R-free*	0.30 (0.47)
Macromolecules	1920
Ligands	6
Protein residues	267
RMS (bonds)	0.012
RMS (angles)	1.54
Ramachandran favoured (%)	89
Ramachandran allowed (%)	6.5
Average B-factor	54.9

Solvent	38.9
---------	------

\*Statistics for the highest-resolution shell are shown in parentheses.

Each MtbThiL monomer consists of 305 residues with two domains (figure 3.18A). Domain A encompasses residues 76 to 176, domain B residue 177-343. Both domains adopt an  $\alpha\beta$ -nucleotide binding fold observed for other ThiL structures as well. The mixed A domain  $\beta$ -sheet has the strand order  $\beta 1\downarrow\beta 5\uparrow\beta 2\downarrow\beta 3\downarrow\beta 4\downarrow$  (figure 3.18B). The A domain  $\beta$ -sheet slightly curves around the two  $\alpha$ -helices  $\alpha 1$  and  $\alpha 2$  lying on the same side of the  $\beta$ -sheet.



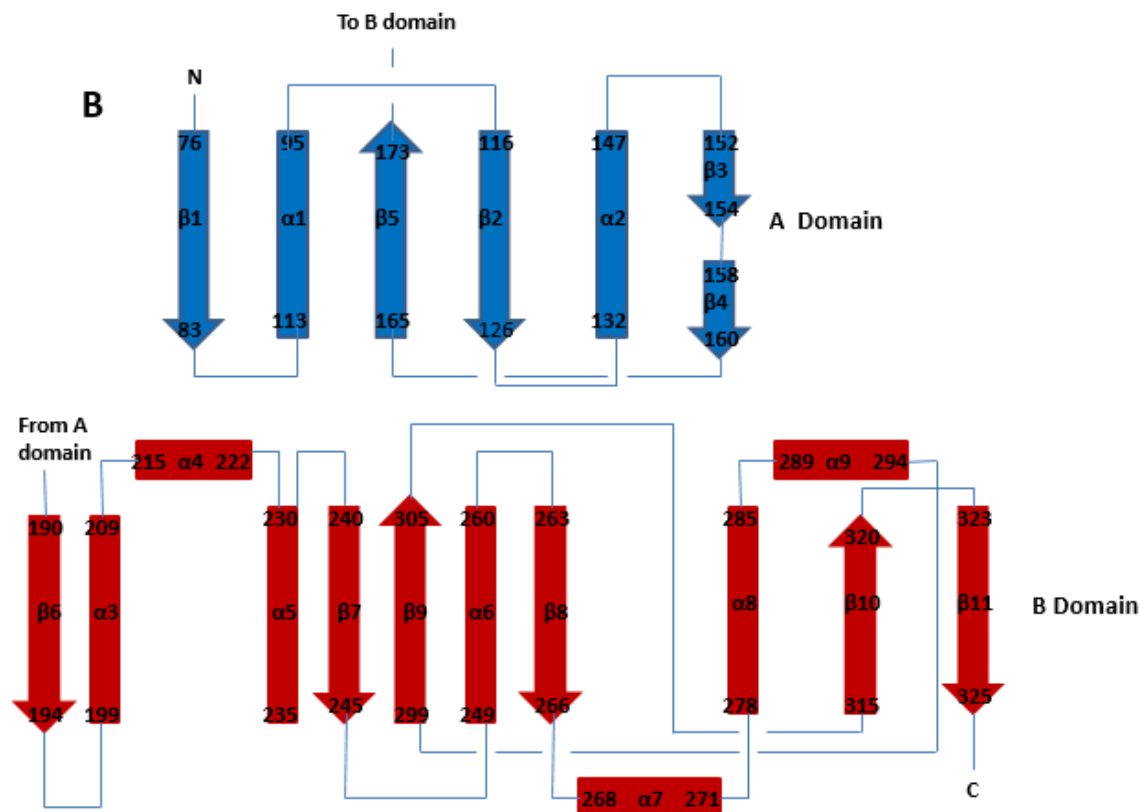


**Figure 3.18: The crystal structure of MtbThiL. (1):** Structural representation of a functional ThiL monomer as found in the asymmetric unit. Domains A and B are respectively coloured blue and red. **Image generated using PyMol. (2):** Topology diagram of MtbThiL. For clarity domains A and B are separated.

The mixed  $\beta$ -sheet of domain B comprises six  $\beta$ -strands with the strand order  $\beta 6 \downarrow \beta 7 \downarrow \beta 9 \uparrow \beta 8 \downarrow \beta 10 \uparrow \beta 11 \downarrow$  (figure 3.18). The  $\beta$ -strands of domain B are generally shorter than those of domain A. The shortest  $\beta$ -strand  $\beta 11$  involves only three residues while  $\beta 9$ , the longest  $\beta$ -strand comprises seven residues. The  $\beta 7$  and  $\beta 10$  strands both have six residues, while  $\beta 6$  and  $\beta 8$  have five and four residues respectively. The helices that flank the  $\beta$ -sheet of the B domain are also shorter than those at the A domain. The domain B  $\beta$ -sheet is flanked on one side by six  $\alpha$ -helices ( $\alpha 3, 4, 6, 7, 8$  and  $9$ ), with only  $\alpha 5$  lying on the other side. The longest  $\alpha$ -helix  $\alpha 6$  is 12 residues in length, while  $\alpha 3, \alpha 4$  and  $\alpha 8$  are respectively eleven, eight and ten residues long. The other helices ( $\alpha 5$  and  $\alpha 9$ ) are both six residues in length, while the shortest helix,  $\alpha 7$  is four residues in length.

### 3.6 Crystallisation of homoserine kinase

The methodology of ThrB crystallisation experiments are outlined in section 2.2.16. Commercial sparse-matrix screens were used to identify crystallization lead conditions. The most promising conditions derived were 15% (w/v) PEG 10 000, 0.2 M MgCl<sub>2</sub>, 0.1 M MES pH 6.8 combined with 15 mg/mL ThrB in 15 mg/mL in 30 mM NaCl, 4 mM MgCl<sub>2</sub>, 1 mM DTT and 50 mM HEPES pH 7.5. Crystallisation experiments at 18°C yielded needle clusters after 4 days (figure 3.19). The crystal size was improved through micro-seeding and by systematically optimising the lead conditions (section 2.2.18).

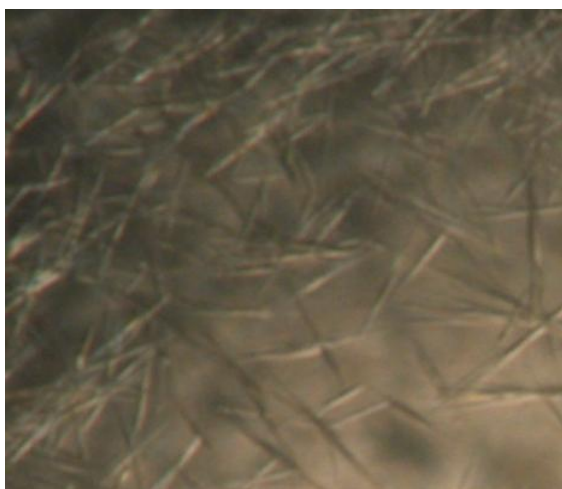


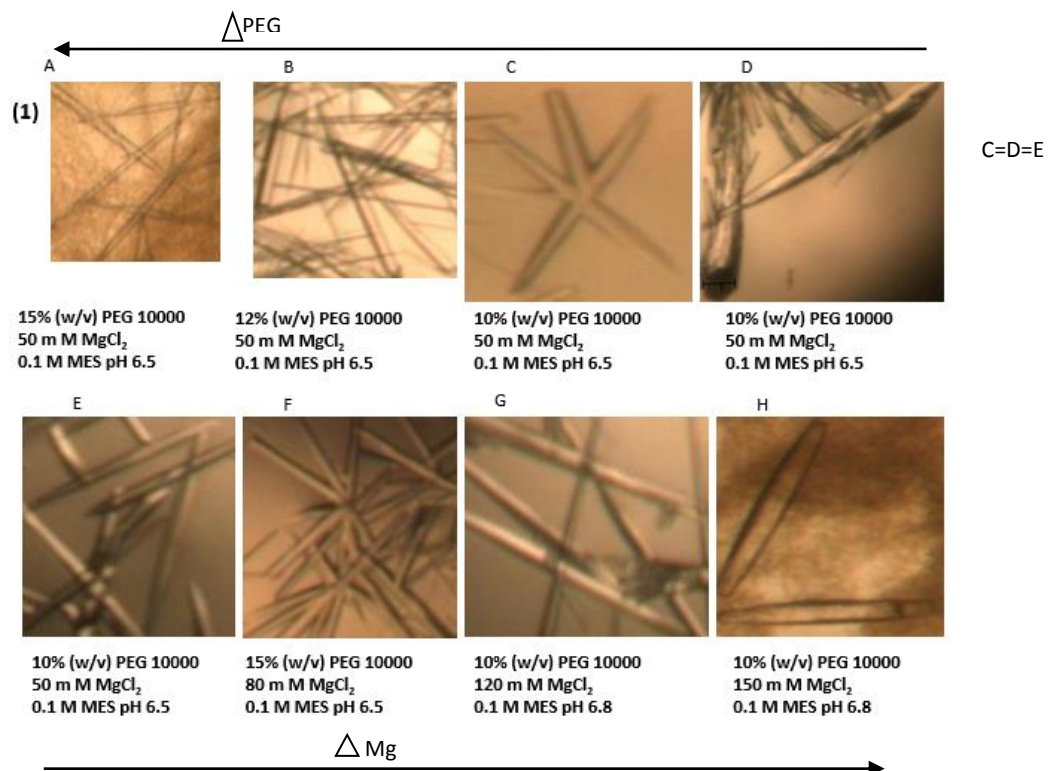
**Figure 3.19: ThrB crystals grown using commercial sparse-matrix screens.** Lead crystallisation conditions: 15% (w/v) PEG 10 000, 0.2 M MgCl<sub>2</sub>, 0.1 M MES pH 7.8.

Varying the ThrB concentration (10 to 18 mg/mL) and temperatures (4, 12 and 18°C) gave rise to crystals similar to those shown in figure 3.20, though crystallisation was significantly slower at 4°C (1 week) as compared to 12 and 18°C (4 days). Conditions were further optimised at 4°C to improve crystal quality. The crystals in figure 3.19 were crushed to produce crystal nuclei for subsequent crystallisation rounds.

#### 3.6.1 Optimisation

Crystallization conditions were optimized by varying the pH (MES pH 5.5, MES pH 6.5 and Tris-HCl pH 7.5), and the concentration of both precipitant PEG 10 000 and the salt MgCl<sub>2</sub>. Crystals of related morphology were obtained at pH 6.5 and 7.5 (figure 3.20), a precipitant concentration between 10 and 15%, and a salt concentration from 30 to 150 mM. Crystals were invariably needle-shaped, reaching a size of ~150 x 35 x 15 μm<sup>3</sup> after

around 4 days. However, crystals did not diffract X-rays to a resolution that would have allowed the structure to be determined.





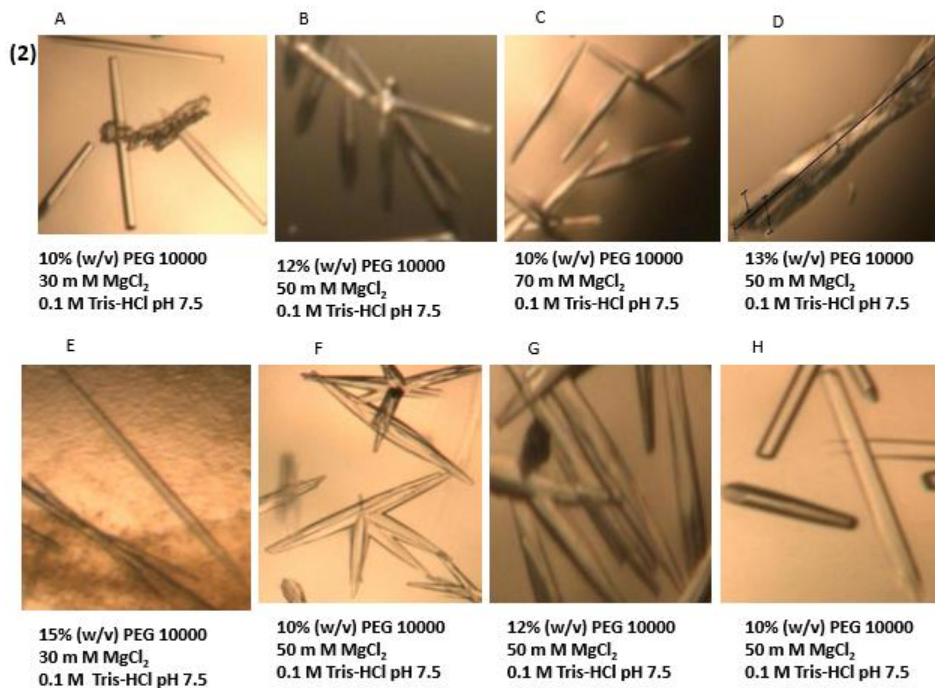


**Figure 3.20: ThrB crystals obtained during optimisation** Crystallisation at (1) pH 6.5, pH 6.8 or pH 7.5 (2) while varying both PEG 10000 and MgCl<sub>2</sub> concentrations. Overall the crystal size and quality could be improved substantially.

## 4 Discussion

The purpose of this research study was to study thiamine phosphate (ThiL) and homoserine kinases (ThrB) from *Mycobacterium tuberculosis* (Mtb). ThiL and ThrB were produced as recombinant His<sub>6</sub>-fusion proteins in *E. coli*. Recombinant proteins were purified using affinity, ion exchange and size exclusion chromatographies. The enzymes were functionally analysed by kinase assays. The proteins were crystallised by hanging-drop, vapour-diffusion and the structure was solved by the molecular replacement.

### 4.1 Production and purification of thiamine-phosphate and homoserine kinases

The production of ThiL and ThrB at 22°C implies that both proteins are better soluble at this temperature. Temperature is known to be a critical parameter for protein production and solubility (Sohoni et al., 2015). Some proteins are best produced and are highly soluble at 37°C, the optimal temperature for the host *E. coli*. Mtb proteins produced in *E. coli* cells, by contrast, require temperatures below 30°C to ensure solubility and efficient

production (Schein and Noteborn, 1988). Optimal yield and solubility for both ThiL and ThrB at 22°C (see section 3.2.5 for ThrB production) thus follows this established trend.

Successful purification of ThiL and ThrB with AXC and SEC implied that both proteins could further be purified with these techniques. The loss of ThiL during AXC could potentially be reduced or overcome by including a small percentage of non-ionic detergent in the protein solution. This was not tested as part of this project though.

#### **4.2 Functional analysis with thiamine-phosphate kinase (ThiL)**

Production of ADP from ATP was used to test for ThiL activity. No ADP was produced in the negative control of the ThiL assay (no ThiL present), while both ADP and TDP were produced in the actual experiment (figure 3.11) indicating that a phosphate group had been transferred from ATP to TMP and signifying that ThiL was catalytically active. Remaining peaks for ATP and TMP peaks in the experimental reaction indicate that the reaction had not run to completion. In fact, product peaks were small compared to those of the substrates implying that the reaction time and/or the balance between enzyme and substrate concentrations still needed to be optimized (Peterson et al., 2007, (Nizam, 2013).

#### **4.3 Functional analysis with homoserine kinase**

As with ThiL, production of ADP by ThrB attests to its catalytic activity (figure 3.12 B). In the absence of the enzyme, no ADP peak was observed and both substrates were required for the phosphate transfer. This implies that the enzyme is needed for the phosphate transfer and both substrates are thus required for the transfer. An ATP peak is absent in this experiment indicating that ATP was quantitatively converted to ADP.

#### **4.4 Crystallisation experiments with thiamine-phosphate kinase**

The needle shaped crystals obtained from initial crystallization of ThiL was a fortunate coincidence as many crystallisation experiments initially yield microcrystals or crystal clusters that require many rounds of optimization to (Luft et al., 2011). The initial ThiL crystals were not directly useful for diffraction experiments, but clearly indicated a worthwhile starting point. First round crystals often are microcrystalline or occur in the form of intergrown needle clusters due to sub-optimal growth conditions. These conditions need to be iteratively and empirically improved to produce larger, single

crystals useful for X-ray diffraction and structure determination (McPherson and Cudney, 2014).

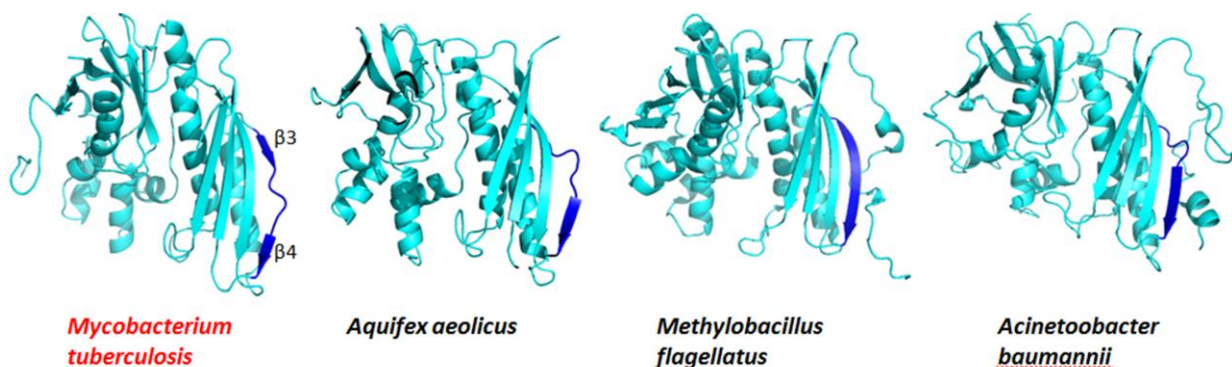
Protein conformational stability enhances crystal growth and lower temperatures reduce conformational flexibility increasing the probability of crystals (Benvenuti and Mangani, 2007). The experiments indicate that this rule similarly applies to ThiL. The crystals were first observed two days after experimental setup producing comparable crystals in number, size and morphology (figure 3.13).

Adjusting other parameters such as pH, precipitant and salt concentration (figure 3.14 and 3.15) increased the size of ThiL crystals. Slight differences in morphology of ThiL crystals obtained at the two different pH does not necessarily imply that the crystals belong to different space groups, as a change in pH can induce different crystal morphologies (Luft et al., 2011). Crystal seeding 1h after the original experimental setup also helped to improve the ThiL crystal quality (figure 3.16) indicating that the timing of seeding is critical for the overall size of protein crystals.

Obtaining quality crystals for X-ray diffraction is thus not a one-step process. Varying one parameter may not suffice to produce better crystals. Instead the critical factors need to be identified and varied in a controlled manner. The protein crystallisation bottleneck thus requires time, dedication and continuous optimization.

#### 4.5 Overall structure of *Mycobacterium tuberculosis* thiamine-phosphate kinase

The overall structure of MtbThiL reveals a nucleotide binding fold in which  $\beta$ -sheets are flanked by  $\alpha$ -helices and loops (figure 3.18). A similar topological organisation has been observed in ThiL structures from other organisms, even though these structures contain most of the first 73 and last 12 residues not present in the MtbThiL structure (Otte et al., 2007) as illustrated by three examples from other bacteria (figure 4.1).



from other prokaryotes: *Aquifex aeolicus* ThiL (PDB code 1VQV-A), *Methylobacillus flagellatus* (PDB code 3MCQ), and *Acinetobacter baumannii* ThiL (PDB code 5DD7-A). The variable region known change its conformation on ATP-binding is highlighted in blue.

The most distinctive feature of MtbThiL is the variable region (VR) coloured blue which varies in conformation. In the ThiL structures, the variable region is the loop that connects  $\alpha 2$  and  $\beta 5$  of the A domain (figure 3.18B). In MtbThiL, part of the loop has adopted a short  $\beta$ -strand ( $\beta 3$ ) between  $\alpha 2$  to  $\beta 4$ . The  $\beta$ -strand  $\beta 4$  of MtbThiL is shorter than in all bacterial structures shown. The residues in the variable region are mostly hydrophobic, consisting of valine, isoleucine, leucine and glycine with the central glycines

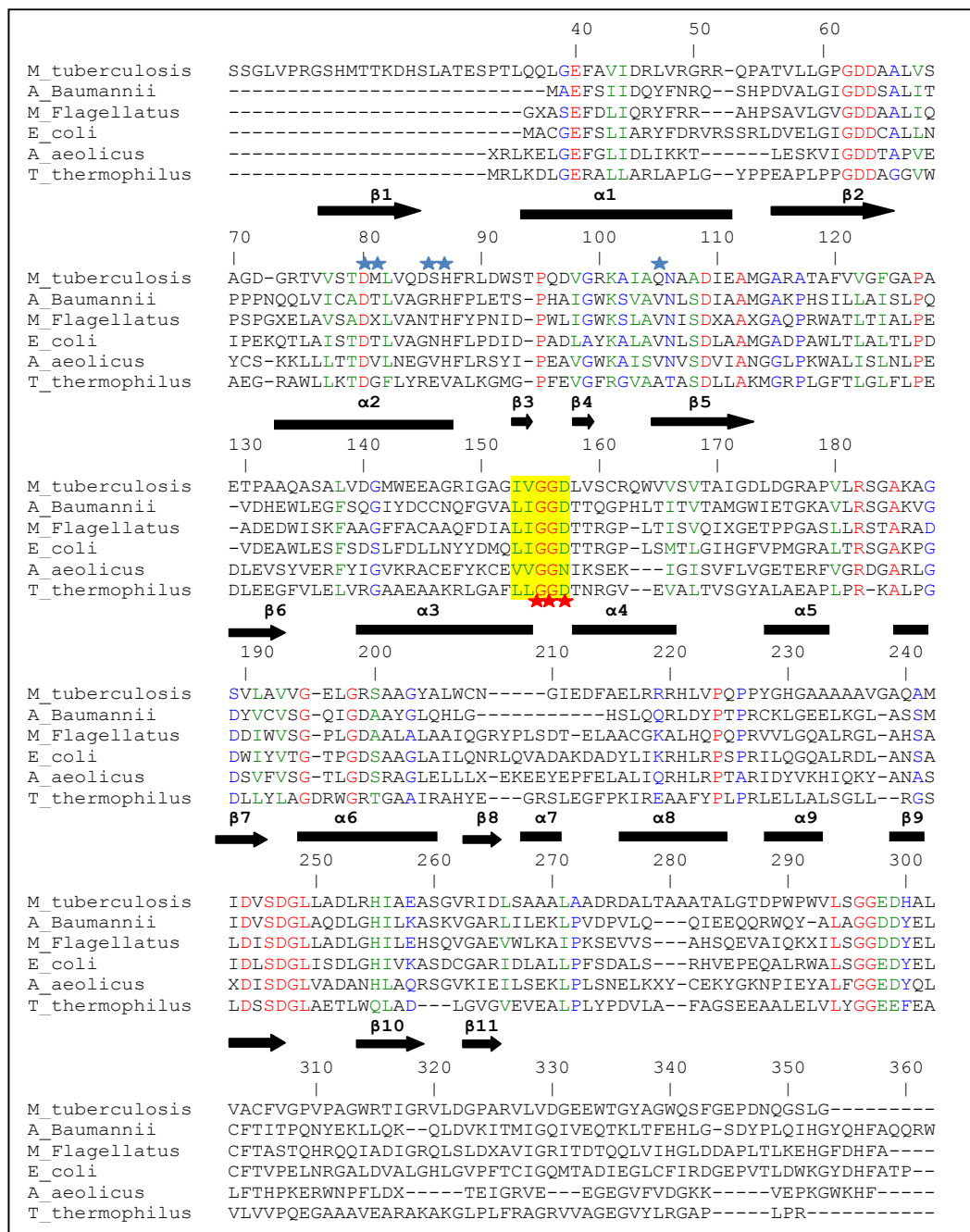


**Figure 4.2: Sequence alignment of MtbThiL with selected ThiL proteins.** MtbThiL secondary structure elements are represented by arrows (β-strands) and rectangles (α-helices). Numbers above the sequence refer to the MtbThiL sequence. Red stars below the sequence indicate amino acid side chains involved in ATP binding; blue stars above the sequence mark amino acid side chains involved in TMP binding. Universally conserved residues are coloured red, while partially conserved residues are coloured blue and green. Residues for the variable region are highlighted in yellow. The structural sequence alignment was done using Pairwise Sequence Alignment (Jaroszewski *et al.*, 2011).

(Gly155 and Gly156) universally conserved. Aspartic acid (Asp157), the only charged residue close to Gly155 and Gly156, is also highly conserved within ThiL proteins (figure 4.2). The ATP-binding area is highly conserved in ThiL structures.

#### 4.6 Superposition of MtbThiL with other ThiL structures

To compare MtbThiL with other ThiL structures in more detail, MtbThiL was superpositioned on *Aquifex aeolicus* ThiL (AaThiL) (PDB code 3C9R, complexed with ATP) and *Acinetobacter baumannii* ThiL (AbThiL) (PDB code 5DD7, complexed with AMP-PNP and TMP).

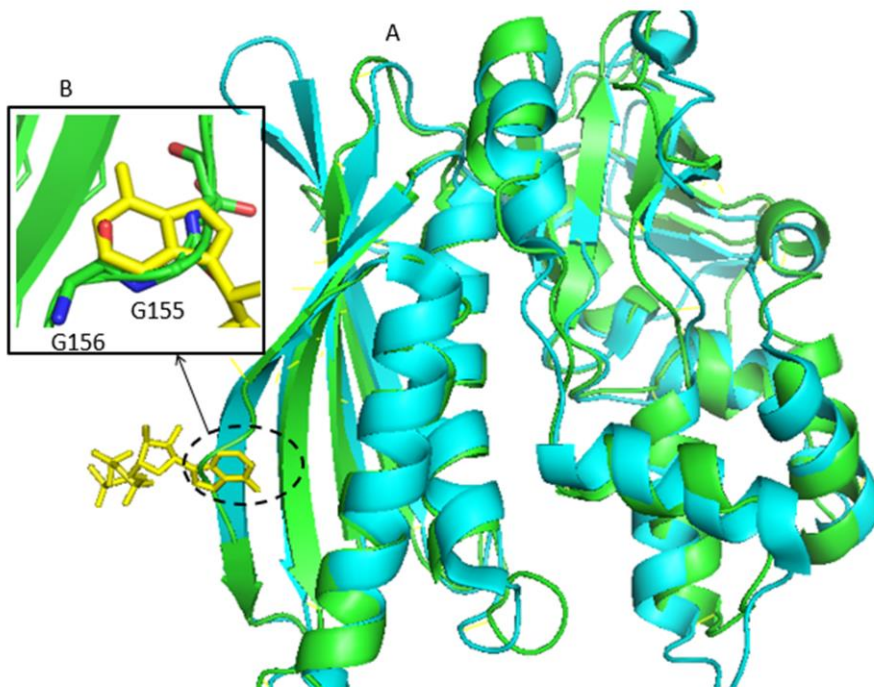


**Figure 4.3: Investigating the substrate binding sites in MtbThiL. A)** Apo-MtbThiL (green) superpositioned on ATP-bound form of *A. aeolicus* ThiL (cyan, PDB code 3C9R, ATP yellow). **B)** A dashed circle marks an enlarged part of MtbThiL near the adenosine portion of ATP/AMP PNP from a superposed AaThiL-ATP complex.

These structures were chosen for superposition because they bind at least one of the substrates allowing the substrates binding sites to be mapped in MtbThiL. The superposition reveals a high degree of similarity of MtbThiL to AaThiL (figure 4.3A). Minor shifts in MtbThiL secondary structure elements are visible relative to the structures of

AaThiL, as is typical for evolutionarily (distantly) related proteins. The MtbThiL crystal structure lacks four secondary structure elements relative to AaThiL. A major conformational change visible in the superposed structures involves the variable region of MtbThiL filling the ATP binding site (figure 4.3A). If an ATP model is placed in its binding site based on related crystal structure, the adenosine base of ATP clashes with Gly155 and Gly156 of the variable region (figure 4.3B). However, this is merely indicative of a relaxed binding site and will not prevent ATP from accessing the active site. Upon ATP binding to its binding site will allow the variable loop to adjust its position, stabilizing the entire protein and resolving any apparent clashes. The structure of MtbThiL is probably in a confined 'open state' – possibly due to crystal packing effects.

#### **4.7 ATP and TMP sub-sites**

Superpositioning the apo-MtbThiL structure, on AaThiL in complex with ATP and AbThiL in complex with AMP-PNP and TMP (figure 4.3A and B) allows the ATP and TMP binding sites to be inferred (figure 4.4). As discussed above, Gly155 and Gly156 clashes with the adenosine of ATP (figure 4.3A and 4.4A). By contrast the TMP binding site easily allows TMP to be modelled in a position equivalent to that of other structures (figure 4.4B). The residues Gly155, Gly156 and Asp157 of the ATP sub-site are conserved in all ThiL family members (see figure 4.2) and are critical for ATP recognition. Asp157 which forms a hydrogen-bond to ATP appears to have both a catalytic and a structural role.

The TMP sub-site, by contrast, includes a number of hydrophilic residues such as Asp80, His87 and Gln105 that bind TMP through hydrogen bonds (figure 4.4B). The sequence alignment (figure 4.2) indicates that Asp80 is conserved in all ThiL proteins implying that it may be involved in catalysis especially as it faces TMP. His87 is replaced in TtThiL, while Met81 and Gln105 are more variable. His87 and Ser86 are optimally placed to function as potential phosphorylation sites, though His87 is nearer to TMP.

To clearly delineate the role of critical residues in the ATP and TMP sub-sites, it may be necessary to substitute sub-site residues. Replacing conserved and some non-conserved residues may identify residues involved in catalysis. At present, no such analyses have been undertaken on any of the published ThiL structures – opening up the opportunity for such studies to be performed on MtbThiL.

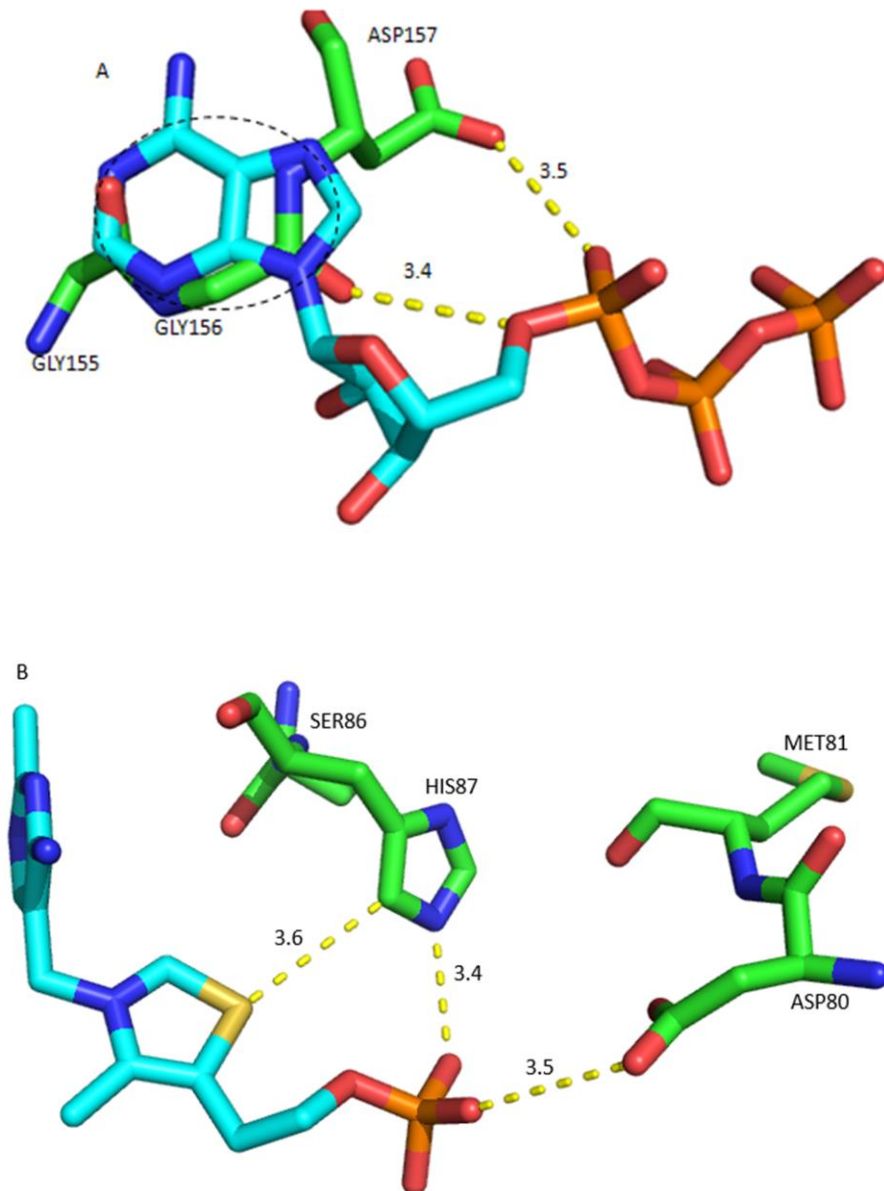


**Figure 4.4: ATP and TMP binding sites.** Substrates ATP (A, cyan) and TMP (B, magenta) were modelled into their respective binding sites by analogy with AaThiL/ATP (PDB code 3C9R) and AbThiL/AMP-PNP/TMP (PDB code 5DD7) complexes. Inferred hydrogen bonds are shown as yellow dashed lines. The Gly155 and 156 blocking the ATP binding site are marked by a dashed circle.



ThiL is a member of the ATP binding superfamily, members of which are believed to use phosphorylated intermediates during catalysis and include the purine biosynthetic enzymes, PurM and PurL, NiFe hydrogenase maturation protein HypE, and selenophosphate synthase SelD. Studies on AaThiL showed that the enzyme does not rely on any reaction intermediates (Kollewe et al., 2004). Presumably this would then also apply to MtbThiL. In addition, because MtbThiL derives from a pathogenic bacterium it may have adapted structurally to its host environment. Possibly the compact nature of the ATP sub-site leading to Gly155 and Gly156 blocking the adenine base of ATP could be one such feature. It may be tempting to speculate that during dormancy, when Mtb is less active and produces less ATP, it would need to regulate the amount of ATP consumed within the cell. One such mechanism could be that the ATP sub-site remains “closed” if the ATP concentration is below a certain threshold and the enzyme is only activated upon ATP binding. Thus despite the substrate (TMP) being present the product TDP would not be produced. The level of vitamin B1 would thus be directly linked to the general metabolic state of the organism.

#### **4.8 Crystallisation experiment with homoserine kinase**

MtbThrB was successfully crystallised (figure 3.20) However, the crystals did not diffract X-rays to a resolution required to solve the crystal structure. A multitude of factors could contribute to this phenomenon including the small size of the crystals, crystal handling and sensitivity of crystals to the cryoprotectant.

## **5 Conclusion**

Functionally active ThiL, 36 kDa, was produced, purified and produced hexagonal crystals belonging to space group  $P6_122$  with one molecule per asymmetric unit. Structurally it is related to ThiL from other organisms. This structure provides the structural basis to develop novel Mtb drugs in the fight against TB.

## 6 Outlook

- Crystallise and solve the structure of MtbThiL in complex with substrates and products.
- Substitute essential MtbThiL residues.  
Do some kinetics on MtbThiL.

## References

- Baer, CE, Iavarone, AT, Alber, T & Sassetti, CM 2014. Biochemical and spatial coincidence in the provisional Ser/Thr protein kinase interaction network of *Mycobacterium tuberculosis*. *Journal of Biological Chemistry*, 289, 20422-33.
- Benvenuti, M & Mangani, S 2007. Crystallization of soluble proteins in vapor diffusion for x-ray crystallography. *Nat. Protocols*, 2, 1633-1651.
- Bhutani, H, Singh, S & Jindal, KC 2005. Drug-Drug Interaction Studies on First-Line Anti-tuberculosis Drugs. *Pharmaceutical Development and Technology*, 10, 517-524.
- Bornhorst, JA & Falke, JJ 2000. [16] Purification of Proteins Using Polyhistidine Affinity Tags. *Methods in enzymology*, 326, 245-254.
- Bourven, I, Simon, S, Bhatia, D, van Hullebusch, ED & Guibaud, G 2015. Effect of various size exclusion chromatography (SEC) columns on the fingerprints of extracellular polymeric substances (EPS) extracted from biological sludge. *Journal of the Taiwan Institute of Chemical Engineers*, 49, 148-155.
- Cadena, AM, Flynn, JL & Fortune, SM 2016. The Importance of First Impressions: Early Events in *Mycobacterium tuberculosis* Infection Influence Outcome. *MBio*, 7, e00342-16.
- Caminero, JA, Sotgiu, G, Zumla, A & Migliori, GB 2010. Best drug treatment for multidrug-resistant and extensively drug-resistant tuberculosis. *Lancet Infect Dis*, 10, 621-9.
- CDC 2006. Emergence of *Mycobacterium tuberculosis* with extensive resistance to second-line drugs--worldwide, 2000-2004. *MMWR Morb Mortal Wkly Rep*, 55, 301-5.
- Du, Q, Wang, H & Xie, J 2011. Thiamin (Vitamin B1) Biosynthesis and Regulation: A Rich Source of Antimicrobial Drug Targets? *International Journal of Biological Sciences*, 7, 41-52.
- Ehrt, S, Rhee, K & Schnappinger, D 2015. Mycobacterial genes essential for the pathogen's survival in the host. *Immunological Reviews*, 264, 319-326.
- Fekete, S, Beck, A, Veuthey, J-L & Guillarme, D 2014. Theory and practice of size exclusion chromatography for the analysis of protein aggregates. *Journal of Pharmaceutical and Biomedical Analysis*, 101, 161-173.
- Ferla, MP & Patrick, WM 2014. Bacterial methionine biosynthesis. *Microbiology*, 160, 1571-1584.
- Fernstrom, A & Goldblatt, M 2013. Aerobiology and Its Role in the Transmission of Infectious Diseases. *Journal of Pathogens*, 2013, 13.
- Fischer, EH 2013. Cellular regulation by protein phosphorylation. *Biochemical and Biophysical Research Communications*, 430, 865-867.
- Gallagher, SR 2001. One-Dimensional SDS Gel Electrophoresis of Proteins. *Current Protocols in Cell Biology*. John Wiley & Sons, Inc.
- Gengenbacher, M & Kaufmann, SHE 2012. *Mycobacterium tuberculosis*: success through dormancy. *FEMS Microbiology Reviews*, 36, 514-532.
- Getahun, H, Matteelli, A, Chaisson, RE & Raviglione, M 2015. Latent *Mycobacterium tuberculosis* Infection. *New England Journal of Medicine*, 372, 2127-2135.
- Gillespie, SH, Crook, AM, McHugh, TD, Mendel, CM, Meredith, SK, Murray, SR, Pappas, F, Phillips, PPJ & Nunn, AJ 2014. Four-Month Moxifloxacin-Based Regimens for Drug-Sensitive Tuberculosis. *New England Journal of Medicine*, 371, 1577-1587.
- Grangeasse, C, Cozzone, AJ, Deutscher, J & Mijakovic, I 2007. Tyrosine phosphorylation: an emerging regulatory device of bacterial physiology. *Trends in Biochemical Sciences*, 32, 86-94.
- Grangeasse, C, Nessler, S & Mijakovic, I 2012. Bacterial tyrosine kinases: evolution, biological function and structural insights. *Philosophical Transactions of the Royal Society of London B: Biological Sciences*, 367, 2640-2655.
- Guo, Y, Bandaru, V, Jaruga, P, Zhao, X, Burrows, CJ, Iwai, S, Dizdaroglu, M, Bond, JP & Wallace, SS 2010. The oxidative DNA glycosylases of *Mycobacterium tuberculosis* exhibit different substrate preferences from their *Escherichia coli* counterparts. *DNA Repair*, 9, 177-190.

- Hansen, SH 2015. General Chromatographic Theory and Principles. *Bioanalysis of Pharmaceuticals*. John Wiley & Sons, Ltd.
- Hao, Q 2004. ABS: a program to determine absolute configuration and evaluate anomalous scatterer substructure. *Journal of Applied Crystallography*, 37, 498-499.
- Hartley, JL, Temple, GF & Brasch, MA 2000a. DNA cloning using in vitro site-specific recombination. *Genome Res*, 10, 1788-95.
- Hartley, JL, Temple, GF & Brasch, MA 2000b. DNA cloning using in vitro site-specific recombination. *Genome Res*, 10, 1788-95.
- Hayashi, M & Nosaka, K 2015. Characterization of Thiamin Phosphate Kinase in the Hyperthermophilic Archaeon *Pyrobaculum calidifontis*. *Journal of Nutritional Science and Vitaminology*, 61, 369-374.
- Horie, K, Sato, Y, Kimura, T, Nakamura, T, Ishihama, Y, Oda, Y, Ikegami, T & Tanaka, N 2012. Estimation and optimization of the peak capacity of one-dimensional gradient high performance liquid chromatography using a long monolithic silica capillary column. *Journal of Chromatography A*, 1228, 283-291.
- Houben, RMGJ & Dodd, PJ 2016. The Global Burden of Latent Tuberculosis Infection: A Re-estimation Using Mathematical Modelling. *PLOS Medicine*, 13, e1002152.
- Hui, YMT, Pillinger, T, Luqmani, A & Cooper, N 2015. Haemophagocytic lymphohistiocytosis associated with Mycobacterium tuberculosis infection. *BMJ Case Reports*, 2015.
- Humphrey, SJ, James, DE & Mann, M 2015. Protein Phosphorylation: A Major Switch Mechanism for Metabolic Regulation. *Trends in Endocrinology & Metabolism*, 26, 676-687.
- Ihara, H, Matsumoto, T, Shino, Y & Hashizume, N 2005. Assay values for thiamine or thiamine phosphate esters in whole blood do not depend on the anticoagulant used. *Journal of Clinical Laboratory Analysis*, 19, 205-8.
- Kardan Yamchi, J, Haeili, M, Gizaw Feyisa, S, Kazemian, H, Hashemi Shahraki, A, Zahednamazi, F, Imani Fooladi, AA & Feizabadi, MM 2015. Evaluation of efflux pump gene expression among drug susceptible and drug resistant strains of Mycobacterium tuberculosis from Iran. *Infection, Genetics and Evolution*, 36, 23-26.
- Kazakevich, Y & LoBrutto, R 2006. Size-Exclusion Chromatography. *HPLC for Pharmaceutical Scientists*. John Wiley & Sons, Inc.
- Kingsbury, JM & McCusker, JH 2010. Fungal homoserine kinase (thr1Delta) mutants are attenuated in virulence and die rapidly upon threonine starvation and serum incubation. *Eukaryot Cell*, 9, 729-37.
- Koch, R 1982. The Etiology of Tuberculosis. *Reviews of Infectious Diseases*, 4, 1270-1274.
- Kollewe, C, Mackensen, AC, Neumann, D, Knop, J, Cao, P, Li, S, Wesche, H & Martin, MU 2004. Sequential autophosphorylation steps in the interleukin-1 receptor-associated kinase-1 regulate its availability as an adapter in interleukin-1 signaling. *J Biol Chem*, 279, 5227-36.
- Kurachi, K, Hosokawa, R, Takahashi, M & Okuyama, H 2014. The potential of glycerol in freezing preservation of turbine oil-degrading bacterial consortium and the ability of the revised consortium to degrade petroleum wastes. *International Biodeterioration & Biodegradation*, 88, 77-82.
- Kwon, YS, Chi, SY, Oh, IJ, Kim, KS, Kim, YI, Lim, SC & Kim, YC 2013. Clinical characteristics and treatment outcomes of tuberculosis in the elderly: a case control study. *BMC Infectious Diseases*, 13, 1-7.
- Lee, JJ, Kan, CM, Lee, JH, Park, KS, Jeon, JH & Lee, SH 2014. Phosphorylation-dependent interaction between a serine/threonine kinase PknA and a putative cell division protein Wag31 in Mycobacterium tuberculosis. *New Microbiol*, 37, 525-33.
- Lee, YV, Wahab, HA & Choong, YS 2015. Potential inhibitors for isocitrate lyase of Mycobacterium tuberculosis and non-M. tuberculosis: a summary. *Biomedical Research Institute*, 2015, 895453.
- Lönnroth, K, Jaramillo, E, Williams, BG, Dye, C & Raviglione, M 2009. Drivers of tuberculosis epidemics: The role of risk factors and social determinants. *Social Science & Medicine*, 68, 2240-2246.

- Luft, JR, Wolfley, JR & Snell, EH 2011. What's in a drop? Correlating observations and outcomes to guide macromolecular crystallization experiments. *Crystal growth & design*, 11, 651-663.
- McCoy, AJ, Grosse-Kunstleve, RW, Adams, PD, Winn, MD, Storoni, LC & Read, RJ 2007. Phaser crystallographic software. *Journal of Applied Crystallography*, 40, 658-674.
- McPherson, A 2004. Introduction to protein crystallization. *Methods*, 34, 254-265.
- McPherson, A & Cudney, B 2014. Optimization of crystallization conditions for biological macromolecules. *Acta Crystallogr F Struct Biol Commun*, 70, 1445-67.
- Metri, R, Hariharaputran, S, Ramakrishnan, G, Anand, P, Raghavender, US, Ochoa-Montaña, B, Higuero, AP, Sowdhamini, R, Chandra, NR, Blundell, TL & Srinivasan, N 2015. SInCRE—structural interactome computational resource for Mycobacterium tuberculosis. *Database*, 2015.
- Molle, V, Gulten, G, Vilcheze, C, Veyron-Churlet, R, Zanella-Cleon, I, Sacchettini, JC, Jacobs, WR, Jr. & Kremer, L 2010. Phosphorylation of InhA inhibits mycolic acid biosynthesis and growth of Mycobacterium tuberculosis. *Mol Microbiol*, 78, 1591-605.
- Nizam, U 2013. Inverse Interpolation: The Rate of Enzymatic Reaction based Finite differences, Formulas for obtaining intermediate values of Temperature, Substrate Concentration, Enzyme Concentration and their Estimation of Errors. *International Journal of Innovation and Applied Studies*, 3, 160-204.
- Nolen, B, Taylor, S & Ghosh, G 2004. Regulation of Protein Kinases: Controlling Activity through Activation Segment Conformation. *Molecular Cell*, 15, 661-675.
- O'Barr, TP & Everett, KA 1971. Effect of l-Homoserine on the Growth of Mycobacterium tuberculosis. *Infection and Immunity*, 3, 328-332.
- Orenstein, EW, Basu, S, Shah, NS, Andrews, JR, Friedland, GH, Moll, AP, Gandhi, NR & Galvani, AP 2009. Treatment outcomes among patients with multidrug-resistant tuberculosis: systematic review and meta-analysis. *The Lancet Infectious Diseases*, 9, 153-161.
- Otte, MM, Woodson, JD & Escalante-Semerena, JC 2007. The Thiamine Kinase (YcfN) Enzyme Plays a Minor but Significant Role in Cobinamide Salvaging in Salmonella enterica. *Journal of Bacteriology*, 189, 7310-7315.
- Pai, M, Behr, MA, Dowdy, D, Dheda, K, Divangahi, M, Boehme, CC, Ginsberg, A, Swaminathan, S, Spigelman, M, Getahun, H, Menzies, D & Raviglion, M 2016. Tuberculosis. *Nature Reviews Disease Primers*, 2, 16076.
- Palomino, J & Martin, A 2014. Drug Resistance Mechanisms in Mycobacterium tuberculosis. *Antibiotics*, 3, 317.
- Palsson-McDermott, EM & O'Neill, LA 2004. Signal transduction by the lipopolysaccharide receptor, Toll-like receptor-4. *Immunology*, 113, 153-62.
- Pereira, SFF, Goss, L & Dworkin, J 2011. Eukaryote-Like Serine/Threonine Kinases and Phosphatases in Bacteria. *Microbiology and Molecular Biology Reviews : MMBR*, 75, 192-212.
- Peterson, Michelle E, Daniel, Roy M, Danson, Michael J & Eienthal, R 2007. The dependence of enzyme activity on temperature: determination and validation of parameters. *Biochemical Journal*, 402, 331-337.
- Petrini, B & Hoffner, S 1999. Drug-resistant and multidrug-resistant tubercle bacilli. *International Journal of Antimicrobial Agents*, 13, 93-97.
- Podinovskaia, M, Lee, W, Caldwell, S & Russell, DG 2013. Infection of macrophages with Mycobacterium tuberculosis induces global modifications to phagosomal function. *Cell Microbiol*, 15, 843-59.
- Prisic, S, Dankwa, S, Schwartz, D, Chou, MF, Locasale, JW, Kang, C-M, Bemis, G, Church, GM, Steen, H & Husson, RN 2010. Extensive phosphorylation with overlapping specificity by Mycobacterium tuberculosis serine/threonine protein kinases. *Proceedings of the National Academy of Sciences*, 107, 7521-7526.
- Prisic, S & Husson, RN 2014. Mycobacterium tuberculosis Serine/Threonine Protein Kinases. *Microbiology spectrum*, 2, 10.1128/microbiolspec.MGM2-0006-2013.

- Rees, WD, Hay, SM & Flint, HJ 1992. Expression of Escherichia coli homoserine kinase in mouse 3T3 cells. *Biochemical Journal*, 281, 865-870.
- Roberts, RJ, Belfort, M, Bestor, T, Bhagwat, AS, Bickle, TA, Bitinaite, J, Blumenthal, RM, Degtyarev, SK, Dryden, DTF, Dybvig, K, Firman, K, Gromova, ES, Gumpert, RI, Halford, SE, Hattman, S, Heitman, J, Hornby, DP, Janulaitis, A, Jeltsch, A, Josephsen, J, Kiss, A, Klaenhammer, TR, Kobayashi, I, Kong, H, Krüger, DH, Lacks, S, Marinus, MG, Miyahara, M, Morgan, RD, Murray, NE, Nagaraja, V, Piekarowicz, A, Pingoud, A, Raleigh, E, Rao, DN, Reich, N, Repin, VE, Selker, EU, Shaw, PC, Stein, DC, Stoddard, BL, Szybalski, W, Trautner, TA, Van Etten, JL, Vitor, JMB, Wilson, GG & Xu, Sy 2003. A nomenclature for restriction enzymes, DNA methyltransferases, homing endonucleases and their genes. *Nucleic Acids Research*, 31, 1805-1812.
- Schein, CH & Noteborn, MHM 1988. Formation of Soluble Recombinant Proteins in Escherichia Coli is Favored by Lower Growth Temperature. *Nat Biotech*, 6, 291-294.
- Selkirk, C 2004. Ion-Exchange Chromatography. In: CUTLER, P. (ed.) *Protein Purification Protocols*. Totowa, NJ: Humana Press.
- Sia, JK, Georgieva, M & Rengarajan, J 2015. Innate Immune Defenses in Human Tuberculosis: An Overview of the Interactions between Mycobacterium tuberculosis and Innate Immune Cells. *Journal of Immunology Research*, 2015, 12.
- Sih, A, Ferrari, MCO & Harris, DJ 2011. Evolution and behavioural responses to human-induced rapid environmental change. *Evolutionary Applications*, 4, 367-387.
- Sohoni, SV, Nelapati, D, Sathe, S, Javadekar-Subhedar, V, Gaikawai, RP & Wangikar, PP 2015. Optimization of high cell density fermentation process for recombinant nitrilase production in E. coli. *Bioresource Technology*, 188, 202-208.
- Song, K-S, Nimse, SB, Cho, NH, Sung, N, Kim, H-j, Yang, J & Kim, T 2015. MTB-DR-RIF 9G test: Detection and discrimination of tuberculosis and multi-drug resistant tuberculosis strains. *Tuberculosis*, 95, 780-785.
- Swartz, M 2010. HPLC DETECTORS: A BRIEF REVIEW. *Journal of Liquid Chromatography & Related Technologies*, 33, 1130-1150.
- Theze, J, Kleidman, L & Girons, IS 1974. Homoserine Kinase from Escherichia coli K-12: Properties, Inhibition by l-Threonine, and Regulation of Biosynthesis. *Journal of Bacteriology*, 118, 577-581.
- Tian, K, Niu, D, Liu, X, Prior, BA, Zhou, L, Lu, F, Singh, S & Wang, Z 2016. Limitation of thiamine pyrophosphate supply to growing Escherichia coli switches metabolism to efficient d-lactate formation. *Biotechnology and Bioengineering*, 113, 182-188.
- Urh, M, Simpson, D & Zhao, K 2009. Affinity chromatography: general methods. *Methods Enzymol*, 463, 417-38.
- Velayati, AA, Masjedi, MR, Farnia, P, Tabarsi, P, Ghanavi, J, ZiaZarifi, AH & Hoffner, SE 2009. Emergence of new forms of totally drug-resistant tuberculosis bacilli: Super extensively drug-resistant tuberculosis or totally drug-resistant strains in iran. *CHEST Journal*, 136, 420-425.
- Weiss, G & Schaible, UE 2015a. Macrophage defense mechanisms against intracellular bacteria. *Immunological Reviews*, 264, 182-203.
- Weiss, G & Schaible, UE 2015b. Macrophage defense mechanisms against intracellular bacteria. *Immunological Reviews*, 264, 182-203.
- Yang, D, Shipman, LW, Roessner, CA, Scott, AI & Sacchettini, JC 2002. Structure of the Methanococcus jannaschii Mevalonate Kinase, a Member of the GHMP Kinase Superfamily. *Journal of Biological Chemistry*, 277, 9462-9467.
- Zemlyanaya, N, Gelmanova, I, Mishustin, S & Janova, G 2015. Estimating costs for treating patients with multi-drug resistant tuberculosis (MDR TB) under the regional tuberculosis control program, Tomsk (Russia). *European Respiratory Journal*, 46.
- Zhang, Y & Yew, WW 2009a. Mechanisms of drug resistance in *Mycobacterium tuberculosis* [State of the art series. Drug-resistant tuberculosis. Edited by C-Y. Chiang. Number 1 in the series]. *The International Journal of Tuberculosis and Lung Disease*, 13, 1320-1330.

- Zhang, Y & Yew, WW 2009b. Mechanisms of drug resistance in *Mycobacterium tuberculosis* [State of the art series. Drug-resistant tuberculosis. Edited by C-Y. Chiang. Number 1 in the series]. *The International Journal of Tuberculosis and Lung Disease*, 13, 1320-1330.
- Zhou, T, Daugherty, M, Grishin, NV, Osterman, AL & Zhang, H 2000. Structure and Mechanism of Homoserine Kinase: Prototype for the GHMP Kinase Superfamily. *Structure*, 8, 1247-1257.
- WHO, 2016. WHO reports on Tb.